Two-stage robust optimization approach for flexible oxygen distribution under uncertainty in integrated iron and steel plants

Sheng-Long Jiang[a,b,*], Gongzhuang Peng[c], I. David L. Bogle[b], Zhong Zheng[a]

[a] *College of Materials Science and Engineering, Chongqing University, Chongqing, 400044, P.R. China*
[b] *Center for Process Systems Engineering, Department of Chemical Engineering, University College London, London WC1E 7JE, U.K.*
[c] *Engineering Research Institute, University of Science and Technology Beijing, Beijing 100083, P.R. China*

Abstract

Optimal oxygen distribution is one of the most important energy management problems in the modern iron and steel industry. Normally, the supply of the energy generation system is determined by the energy demand of the manufacturing processes. However, the balance between supply and demand fluctuates frequently, owing to the uncertainty arising in the manufacturing processes. In this study, we developed an optimal oxygen distribution considering uncertain demands and proposed a two-stage robust optimization (TSRO) model with a budget-based uncertainty set that protects the initial distribution decisions with low conservatism. The main goal of the TSRO model is to make "wait-and-see" decisions, maximizing energy profits, and make "here-and-now" decisions, minimizing operational stability and surplus/shortage penalty. To represent the uncertainty set of energy demands, we developed (1) a Gaussian process-based time-series model, to forecast the demand intervals for continuous processes, and (2) a capacity-constrained scheduling model, to generate multi-scenario demands for discrete processes. We perform extensive computational studies on TSRO and its components using well-synthesized instances from historical data. The results of model validation and analysis are promising and demonstrate that our approach is well adapted to solving industrial cases under uncertainty.

Keywords: oxygen distribution, iron and steel industry, robust optimization, demand forecasting, process scheduling, machine learning

1. Introduction

Energy plays a vital role in the plant-wide optimization of manufacturing systems, aiming to achieve a carbon-neutral economy [1]. However, two major challenges are faced by most energy intensive manufacturers: (1) rising energy costs and (2) strict emission requirements. These challenges are particularly severe in the iron and steel industry because it is the second-largest energy consumer in global industrial sectors [2]. Oxygen is one of the most fundamental energy resources in integrated iron and steel plants because some processes require a significant amount of oxygen gas, e.g., steelmaking via basic oxygen furnace (BOF), ironmaking via blast furnace (BF). Moreover, oxygen is also a critical health resource, especially during the COVID-19 pandemic. Therefore, optimal decisions on oxygen distribution can significantly enhance productivity and energy efficiency, as well as indirectly contributing to mitigating the public health crisis.

In an integrated iron and steel plant, the oxygen energy system is mainly composed of three subsystems (as illustrated in Fig. 1): an oxygen-generating system (OGS), oxygen storage system (OSS) and oxygen user system (OUS). OGS has a set of air separation units (ASUs) that simultaneously separate atmospheric

*Corresponding author: +86 13520412520
Email addresses: sh.l.jiang.jx@gmail.com (Sheng-Long Jiang), gzpeng@ustb.edu.cn (Gongzhuang Peng), d.bogle@ucl.ac.uk (I. David L. Bogle), drzhongz@hotmail.com (Zhong Zheng)

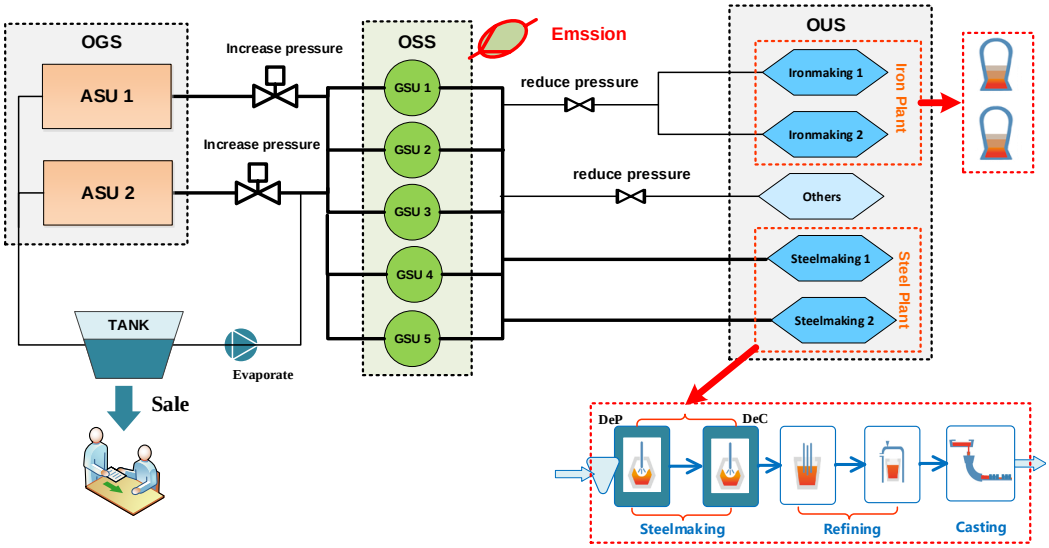

Fig. 1: Oxygen supply and demand system in a integrated iron and steel plant

air into pure gases, typically including nitrogen, oxygen and argon. The liquid oxygen is poured into a tank, and the gaseous oxygen flows into the supply network connected to the OUS. OSS includes a pipeline network that supplies high-pressure gas to each user and some oxygen gasholder units (GSUs), working as a buffer between supply and demand. OUS mainly comprises ironmaking, steelmaking processes and other processes, which consume gaseous oxygen at different pressures. During routine production, the ironmaking and steelmaking processes consume most of the oxygen, i.e., approximately 40% for ironmaking and 50% for steelmaking. In an integrated iron and steel plant, the decision support system, called energy management system (EMS), focuses on determining the optimal operational parameters, balancing the supply from the OGS and the demand from the OUS.

During the oxygen distribution horizon, we assume that: (1) other gases, including Nitrogen and argon, are sufficient. The distribution of oxygen cannot affect the EMS distributing other gaseous energy from the OGS to the OUS. (2) The OGS operates under normal conditions, and no machine breakdown occurs. (3) Liquid oxygen is a type of recoverable energy, and is only used when any ASU in OGS breaks down or the demand from OUS surges. Most approaches to handle oxygen distribution seek optimal operations and assume all parameters associated with manufacturing and energy are fully known. However, the balance between oxygen supply and demand often suffers from environmental and systematic uncertainty because of unforeseen events or unobservable factors, e.g., the dynamic arrival of materials and duration variation of processes. In practice, this means that the energy distribution decisions made by the EMS may not fulfil the predesigned balance. Therefore, how to distribute oxygen under uncertainty is a critical issue for the EMS achieving safety, stable and smart management.

The remainder of this paper is organized as follows. In Section 2, we review energy optimization models in iron and steel plants and the robust optimization (RO) technique under uncertainty. In Section 3, the deterministic model for optimal oxygen distribution and its uncertainty model using the two-stage robust optimization (TSRO) approach are proposed. Sections 4 and 5 are devoted to developing a time series and process scheduling model, respectively, to describe the uncertainty of oxygen demand, respectively. Section 6 presents computational studies that verify the effectiveness of the proposed approaches. The final section provides conclusions and future perspectives of the study.

2. Literature review

The iron and steel manufacturing system is integrated with the energy and material flows, each of which restricts and promotes the other [3]. Gaseous oxygen provides energy to the manufacturing processes in OUS to perform reactions or manufacturing, and the operations of OGS and OSS are guided by the consumption demand of the manufacturing processes [4]. Therefore, a good trade-off between manufacturing and energy systems is essential for sustainable manufacturing in modern iron and steel plants [5]. Many scholars and practitioners have emphasized that this challenge can be addressed from the perspective of energy efficiency and demand-side management [6]. Meanwhile, continuous advances in mathematical modeling and artificial intelligence (AI) technologies have provided new opportunities to address the optimal distribution problem in the EMS of iron and steel plants.

Most studies on the energy distribution in iron and steel plants mainly focused on making an optimal distribution with fixed demands using mixed-integer linear programming (MILP). Kong et al. [7] and Zhao et al. [8] proposed MILP models simultaneously considering both operational and environmental factors. Zhao et al. [9] also studied a distribution model of by-product gas system under time–of–use tariff. Zhang et al. [10] studied a optimization model for steam power system. Recent studies also stressed the importance of optimal oxygen distribution in iron and steel plants. Zhang et al. [11] formulated an optimal oxygen distribution problem with a MILP model that simultaneously minimized the emission, pressure, liquefied, steam, and setup costs. Zhang et al. [12] proposed a simultaneous multi-period distribution model that involves adjustments variables on the supply side, e.g., oxygen generation rate of each ASU and the compression rate of the compressor.

The optimal energy distribution can be achieved by exploring the flexibility of demand from the integrated perspective of energy and material flows [13]. Zeng et al. [14] proposed an improved MILP-based optimal distribution model by introducing new decision variables called consumption rates of by-product gases. Nolde and Morari [15] proposed a MILP-based scheduling solution to minimize the penalty caused by electricity overconsumption and underconsumption. Castro et al. [16] proposed a resource–task network to model an energy-constrained scheduling problem in iron and steel plants; moreover, they studied the influence of fluctuating energy prices on operations and economic benefits. Hadera et al. [17] developed a continuous-time MILP model that simultaneously optimized steelmaking scheduling and an electricity load commitment. Specially, the demand side of oxygen distribution integrates both continuous and discrete processes, each of which has different consuming characteristics. The oxygen demand of an ironmaking process can be controlled by a continuous variable called the flow rate [18]. The oxygen demand of a steelmaking process is always adjusted by implementing optimal process scheduling. For example, Xu et al. [19] proposed an optimal steelmaking scheduling method to reduce fluctuations in oxygen demand.

More recently, the emerging AI technologies, such as machine learning and swarm intelligent, open up new ways to further study complex energy distribution problems in integrated iron and steel plants. Xi et al. [20] developed machine learning-based surrogate models for different processes and applied a particle swarm optimization (PSO) algorithm to find the optimal solution under operating constraints. AI is also a powerful tool to investigate the optimal energy distribution under uncertainty. Because the gasholder serves as a buffer during the distribution procedure, Zhang et al. [10] and Zhao et al. [21] improved the least-squares support vector machine (LS-SVM) approach to forecast the gasholder level with noise. Zhao et al. [22] proposed a AI-based optimization method that forecasted the objective intervals via a Gaussian kernel-based learning model in the offline stage and implemented a time-horizon rolling MILP model in the online stage. Jin et al. [23] employed directed acyclic graphs to construct the causal relationship of a converter gas system, found the best scheduling solution via a PSO algorithm, and developed a gas scheduling software system [24]. Some practitioners also attempted to optimize oxygen distribution using AI techniques. Han et al. [25] applied a granular-computing-based model to forecast the oxygen/nitrogen requirements and developed a MILP-based optimization model to distribute oxygen. Han et al. also [26] employed an LS-SVM to fit the relationship between the energy load and electricity cost of an ASU, and proposed a PSO algorithm to find the optimal distribution.

To address the uncertainty in an optimal distribution model, we naturally employ stochastic programming (SP) or robust optimization (RO) to model the decision process. Unlike SP, which knows probabilistic

information, RO only assumes that the decision-maker has little knowledge about the underlying uncertainty (except for its upper and lower bounds) and seeks an optimal solution that covers the worst-case cost within a well-synthesized uncertainty set. As early as 1973, Soyster [27] began to study the robust linear programming problem. However, the RO technique was not widely used until Ben-Tal and Nemirovski [28] proposed a seminal theory. Recent literature survey by Virginie Gabrel et al. [29] and Bram Gorissen et at. [30] indicate that RO has been widely used in transportation, supply chain, and process scheduling; moreover, RO has been receiving increased attention as a modelling technique for energy systems. The essence of RO is to identify an optimal solution with strictly safe protection. However, it is too conservative to apply in practice, because all uncertain parameters are unlikely to reach the worst-case simultaneously. Therefore, this shortage motivates practitioners in the RO community to seek alternative uncertainty sets with probabilistic guarantees, such as ellipsoidal, polyhedral, and budget-based sets [30]. The budget-based uncertainty set, which was proposed in [31], intuitively interprets uncertainty for a risk-averse decision-maker who might flexibly adjust the level of risk aversion by tuning the so-called budget of uncertainty. Notably, this representation of uncertainty is sufficiently general to represent interactions with energy management and can be easily interpreted by decision-makers.

According to the previous studies, recent studies tended to focus on the uncertain energy distribution problem in integrated iron and steel plants. They assumed the key factor (i.e. gasholder level) or relationship between generation and consumption of the uncertainty are predictable and sought optimal decisions with deterministic optimization models. However, a large variety of unforeseen events in the realistic manufacturing and energy systems may affect the prediction accuracy and the feasibility of optimization models. To construct a more legitimate model, we model the oxygen distribution problem with uncertain demand (only knows limited information) and explore the flexibility on the demand side to form uncertainty sets. The contributions of this paper can be summarized by the following aspects:

- Build an optimal oxygen distribution model considering flexible demands for continuous and discrete processes. The details are presented in Section 3.2.
- Derive a TSRO model with a budget-based uncertainty set that has deeper insight into optimal oxygen distribution. The details are presented in Section 3.3.
- Develop a time-series model via machine learning to forecast the oxygen demands of continuous processes. The details are presented in Section 4.
- Develop a process scheduling model to form the oxygen demands of discrete processes. The details are presented in Section 5.

Nomenclature

Sets,Indices

R, r Suppliers of OGS.

Q, q Users of OUS,and Q^N, Q^E repectively denote continuous and discrete user sets.

L, l Time units of the process scheduling horizon.

Θ, θ Time periods of oxygen distribution, $\Theta_\theta = 1, \ldots, \theta$.

T, t Time horizons of the energy demand time series.

S, s Scenario set of discrete engery demands.

G, g Stage set and index of a steelmaking work.

M_g, m Machine set and index in stage g.

J, j Job set relased into a steel plant.

$A, (g, j)$ Task set processed in a steel palnt, and $A_{g,j}$ is the task of job j processed on stage g.

H, h Batch set and index groupped by the released jobs.

Parameters of oxygen distribution model

$\omega_r^{\min}$ Minimum load of oxygen generator r, $\left[Nm^3\right]$

$\omega_r^{\max}$ Maximum load of oxygen generator r, $\left[Nm^3\right]$

$\hat{\omega}_{\max}$ Maximum deviation of oxygen load between period $(\theta - 1)$ and θ, $\left[Nm^3\right]$

$\rho_q^{\min}$ Minimum adjustment rate of oxygen user q, [%]

$\rho_q^{\max}$ Maximum adjustment rate of oxygen user q, [%]

GV_θ Volume of gas storage at time period θ, $\left[Nm^3\right]$

$GV_{\min}$ Minimum level of the oxygen storage, $\left[Nm^3\right]$

$GV_{\max}$ Maximum level of the oxygen storage, $\left[Nm^3\right]$

GV_{mid} Middle level of the oxygen storage, $\left[Nm^3\right]$

$d_{q,\theta}$ Demand of user q at period θ, $\left[Nm^3\right]$

$\bar{d}_\theta$ Nominal demand of at period θ, $\left[Nm^3\right]$

$\hat{d}_\theta$ Maiximal demand deviation at period θ, $\left[Nm^3\right]$

ξ_θ Scale factor for uncertain demand at period θ, $\left[Nm^3\right]$

Γ_θ Time-variant budget of uncertainty set

Parameters of forcasting model

λ_t Total oxygen demand at distribution horizon t, $\left[Nm^3\right]$

y_t State variable at distribution horizon t

ε_t White noise of oxygen demand during distribution horizon t

TL Time lags of state space model in time series

n Size of training input in time series

Parameters of scheduling model

$PT_{g,j}$ Processing time of task $A_{g,j}$, $[min]$

$TT_{g,gg}$ Transfer time between stage g and gg,$[min]$

SU_h Setup time of batch h, $[min]$

$ES_{g,j}$ Earliest starting time point of task $A_{g,j}$

$LF_{g,j}$ Latest finish time point of task $A_{g,j}$

$WL_s^{\max}$ Maximum capacity of oxygen in the q^{th} scenario of the primary steelmaking stage

Variables

$\omega_{r,\theta}$ Continuous variable of oxygen distribution model, which represents load of gaseous oxygen of supplier r at time period θ, Nm^3

$\rho_{q,\theta}$ Continuous variable of oxygen distribution model, which represents oxygen adjustment rate of of user q at time period θ

δ_θ Continuous variable of oxygen distribution model, which represents deviation from the gasholder level to its middle level at time period θ, Nm^3

ϵ_θ Continuous variable of oxygen distribution model, which represents volume of surplus or shortage volume at time period θ, Nm^3

z_s Binary variable of oxygen distribution model, which is equal to 1 if and only if the steelmaking schedule of the s^{th} scenario is selected

$x_{g,j,l}$ Binary variable of the scheduling model, which is equal to 1 if and only if task $A_{g,j}$ is in-process at time t

3. Optimal oxygen distribution model

3.1. Oxygen distribution in iron and steel plants

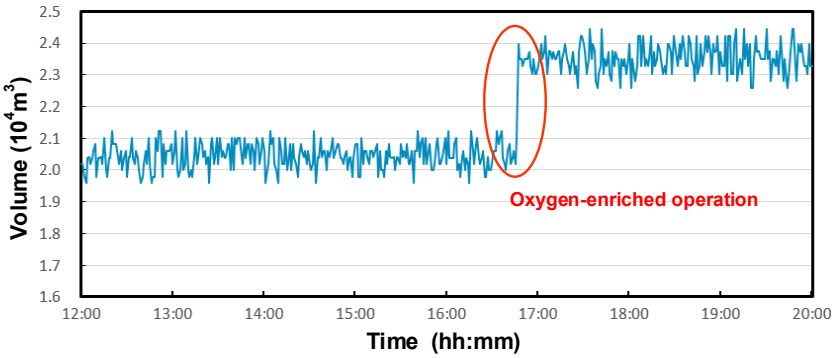

(a) in the ironmaking process

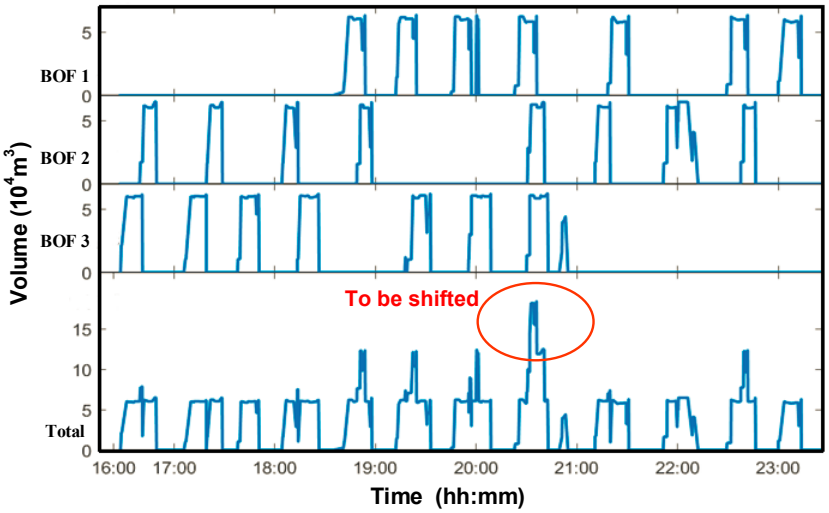

(b) in the steelmaking process

Fig. 2: Actual oxygen consumption on the demand side

As illustrated in Fig. 1, we assume that a set of ASUs ($R = \{1, \ldots, r, \ldots, |R|\}$) exists in OGS and a set of users ($Q = \{1, \ldots, q, \ldots, |Q|\}$) exists in OUS. To implement an optimal decision for oxygen distribution, we divide the a distribution horizon into multiple time periods ($\Theta = \{1, \ldots, \theta, \ldots, |\Theta|\}$) and balance supply and demand in each period by setting operational parameters for both sides. On the supply side, the generation load of each ASU ($\omega_{r,\theta}$) can be controlled to produce the oxygen volume. On the demand side, there are two approaches for adjusting the oxygen demand. In the ironmaking process, oxygen-enriched hot air is continuously pumped into the BF to produce molten iron [32]. The oxygen level in hot air can be adjusted according to the oxygen supply. In the steelmaking process, multiple machines may work simultaneously. Scheduling simultaneous processing tasks helps to avoid overloading or underloading [33]. These policies are verified by the actual data from the EMS, as shown in Fig. 2. Therefore, we introduce two variables to define flexibility on the demand side.

- Adjustment rate (ρ_q), which represents the oxygen level in the hot air against the standard value.
- Scheduling scenario (s), which represents the schedule under a specific limit of the multiple simultaneous processing tasks (so-called capacity) in the steelmaking process.

However, the oxygen demand in each period ($d_{q,\theta}$) may be affected by unknown factors, and cannot be precisely estimated. At the beginning of the first period, the EMS must consider potential uncertainties in the future, to make robust decisions and achieve a balance between supply and demand. When any demand in the OUS varies during period θ, the EMS should control the gasholder level to build a new balance between supply and demand. If these actions are ineffective, the gas in the OSS will be in shortage or surplus, which incurs extra costs. Considering the demands under uncertainty, we propose a TSRO model for flexible oxygen distribution, as shown in Fig. 3. In the first stage, we determine the operational parameters of the supply and demand sides. In the second stage, we choose an adjustment policy according to the status of the gasholder.

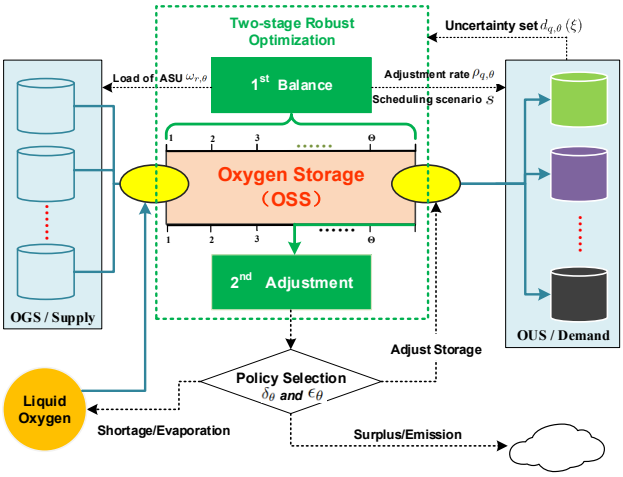

Fig. 3: TSRO model for flexible oxygen distribution

In the following subsections, we formulate a deterministic optimal oxygen distribution model involving flexible demands and develop a TSRO model which only knows limited information of demands.

3.2. Deterministic model with flexible demands

3.2.1. Objectives

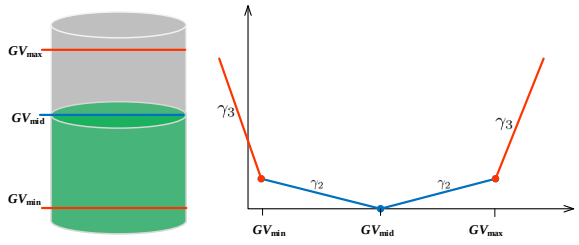

Fig. 4: piecewise function for stability and penalty

In the balance stage, the EMS first needs to increase the energy profit by maximizing the total load of the OGS within the distribution horizon. In the adjustment stage, the gasholder level of the OSS fluctuates frequently owing to varying demands. When the gasholder level is greater than $GV_{\max}$, the surplus results in environmental pollution. When the gasholder level is less than $GV_{\min}$, the shortage incurs an extra cost by evaporating liquid oxygen into the gasholder. Therefore, the middle level GV_{mid} of the gasholder (1/2 between $GV_{\min}$ and $GV_{\max}$, as shown in Fig. 4) reflects the best compromise between shortage and surplus [8]. Thus, to ensure efficiency in reducing the risk of a gas system imbalance, affecting the manufacturing

processes, the gasholder level should be retained approximately at the middle level. In other words, the decision objective f includes the maximizing energy profit f_1, the minimizing gasholder deviation f_2 and surplus/shortage penalty f_3.

$$\begin{aligned} \max f &= f_1(\omega) - f_2(\delta) - f_3(\epsilon) \\ &= \gamma_1 \sum_{r\in R}\sum_{\theta\in\Theta} \omega_{r,\theta} - \gamma_2 \sum_{\theta\in\Theta} |\delta_\theta| - \gamma_3 \sum_{\theta\in\Theta} |\epsilon_\theta| \end{aligned} \tag{1}$$

where δ_θ denote the deviation from GV_{mid}, ϵ_θ denote the volume of shortage and surplus; γ_1 , γ_2 and γ_3 denotes the coefficient of each objective.

3.2.2. Constraints

1) Operational constraints: In the balance stage, the load ($\omega_{r,\theta}$) of ASU r in period θ and the adjustment rate (ρ_q) of user q on the continuous demand side are limited within the specified intervals (Eqs.2 and 3). Only one scenario (z_s) for the demands of discrete users can be selected (Eq.4).

$$\omega_r^{\min} \le \omega_{r,\theta} \le \omega_r^{\max} \qquad \forall r \in R. \wedge \theta \in \Theta \tag{2}$$

$$\rho_q^{\min} \le \rho_q \le \rho_q^{\max} \qquad \forall q \in Q^N \tag{3}$$

$$\sum_{s\in S} z_s = 1 \qquad \forall z_s \in \{0,1\} \tag{4}$$

2) Ramp constraints: In the balance stage, the load deviation of a ASU between two periods ($\theta-1$ and θ) needs to be limited.

$$|\omega_{r,\theta} - \omega_{r,\theta-1}| \le \hat{\omega}_{\max} \qquad \forall r \in R, \theta \in \Theta \setminus \{1\} \tag{5}$$

3) Flexible demands: The total energy demand in each period (d_θ) is determined by the adjustment rates (ρ_q) of the continuous users and the selected scenario (z_s) of the discrete users.

$$d_{q,\theta}(\rho, z) = \sum_{q\in Q^N} \rho_q d_{q,\theta} + \sum_{q\in Q^E} z_s d^s_{q,\theta} \quad \forall\theta \in \Theta \tag{6}$$

4) Gasholder level: The oxygen generated at the end of the $(\theta-1)^{st}$ period flows into OSS at the beginning of the θ^{th} period, that is, all generated gas flows smoothly. According to the material equilibrium relationship proposed by Zhang et al. [12], the total generated oxygen and user demand equals the storage change in the OSS. Hence $GV_\theta - GV_{\theta-1} = \sum_{r\in R}\omega_{r,\theta} - d_\theta(\rho, z)$. Because the surplus demand causes emission and shortage of oxygen cause stock-out, we introduce a variable ϵ_θ to denote the volume of surplus or shortage, respectively. Next, we can re-express the gasholder level (GV_θ) using the following closed-form equation.

$$GV_\theta = GV_0 + \sum_{r\in R}\sum_{\tau\in\Theta_\theta} \omega_{r,\tau} - \sum_{\tau\in\Theta_\theta} \epsilon_\theta - \sum_{\tau\in\Theta_\theta} d_\tau(\rho, z) \quad \forall\theta \in \Theta \tag{7}$$

where GV_0 denotes the initial gasholder level.

5) Capacity constraints: The pressure of the OSS is commonly limited by its maximum and minimum values. According to the conversion relationship proposed by Zhang et al. [12], we define the safety volume of the OSS within a specific range, $[GV_{\min}, GV_{\max}]$. Thus, the capacity restrictions are represented using Eqs.(8)

$$GV_{\min} \le GV_\theta \le GV_{\max} \quad \forall\theta \in \Theta \tag{8}$$

6) Deviation definition: In the θ^{th} period, the deviation between the current gasholder level and middle level can be expressed using following equality.

$$\delta_\theta = GV_\theta - GV_{\text{mid}} \tag{9}$$

7) Nonlinearity transformation: It can be easily observed that the nonlinearity of the model derives from Eqs.1 and 5. We introduce auxiliary variables: δ_θ^- and δ_θ^+; ϵ_θ^- and ϵ_θ^+; $\omega_{r,\theta}^-$ and $\omega_{r,\theta}^+$. Next, we let them satisfy following constraints:

$$\begin{cases} \delta_\theta = \delta_\theta^+ - \delta_\theta^- \\ |\delta_\theta| = \delta_\theta^+ + \delta_\theta^- \\ \delta_\theta^- \geq 0, \delta_\theta^+ \geq 0 \end{cases} \quad \forall \theta \in \Theta \tag{10}$$

$$\begin{cases} \epsilon_\theta = \epsilon_\theta^+ - \epsilon_\theta^- \\ |\epsilon_\theta| = \epsilon_\theta^+ + \epsilon_\theta^- \\ \epsilon_\theta^- \geq 0, \epsilon_\theta^+ \geq 0 \end{cases} \quad \forall \theta \in \Theta \tag{11}$$

$$\begin{cases} \omega_{r,\theta} - \omega_{r,\theta-1} = \omega_{r,\theta}^+ - \omega_{r,\theta}^- \\ |\omega_{r,\theta} - \omega_{r,\theta-1}| = \omega_{r,\theta}^+ + \omega_{r,\theta}^- \\ \omega_{r,\theta}^- \geq 0, \omega_{r,\theta}^+ \geq 0 \end{cases} \quad \forall \theta \in \Theta \setminus \{1\} \tag{12}$$

3.2.3. Abstract model

Observed the deterministic model (1)-(12), we found that only Eqs.(6-9) directly link with uncertain demands. To simplify the notations and facilitate model analysis, we used set $\mathcal{D}$ to define feasible region confirmed by Eqs.(2-5, 10-12), and re-write Eqs.(6-9) to canonical inequities. By dimensionality reduction, we complete the following abstract optimal oxygen distribution (AO2D) model.

$$(\text{AO2D}) \begin{cases} \max & f_1(\omega) - f_2(\delta) - f_3(\epsilon) \\ s.t. & \sum_{\tau=1}^{\theta} (\omega_\tau + d_\tau(\rho, z) + u_\tau(\delta, \epsilon)) \leq v_\theta \\ & \forall \theta \in \Theta, \omega \in \mathcal{D}^\omega, (\rho, z) \in \mathcal{D}^{\rho \times z}, (\delta, \epsilon) \in \mathcal{D}^{\delta \times \epsilon} \end{cases} \tag{13}$$

where ω_θ represents two-index variable $\omega_{r,\theta}$; $d_\theta(\rho, z)$ denotes demand in each period based on variables ρ_q and z_s, $u_\tau(\delta, \epsilon)$ expresses relationship between variables δ_θ and ϵ_θ, v_θ is the right-hand-side constants , respectively.

3.3. Robust model with limited information

According to the simplified formulation (13), AO2D model can be identified as a variant of the multi-period inventory management problem with multi-stage decision process. In this study, we assume that the oxygen demand of each user is uncertain, and closely follows the idea of RO proposed by Bertsimas and Sim [31] and Bertsimas and Thiele [34]. Subsequently, the dynamic decision process is divided into two stages. (1) In the first stage, we determine here-and-now variables (i.e., load of ASU $\omega_{r,\theta}$, adjustment rate ρ_q, and scenario selection y_s) with foresight. (2) In the second stage, we determine wait-and-see variables in hindsight, where some uncertain demands are revealed. To make the worst-case RO less conservative, we also introduce a budget-based uncertainty set that minimizes the deviation to the best profit in a certain scenario. Consequently, we develop the TSRO model using the following three steps.

3.3.1. Step 1: Construct an uncertainty set of demands

In this study, we assume that oxygen demand d_θ is an uncertain variable, for which only the nominal value and bound are known. Let $[\bar{d}_\theta - \hat{d}_\theta, \bar{d}_\theta + \hat{d}_\theta]$, where $\bar{d}_\theta$ is the nominal demand and $\hat{d}_\theta$ is the maximal deviation. Next, we define a scale factor of the uncertain variable, $\xi_\theta = (\hat{d}_\theta - \bar{d}_\theta)/\hat{d}_\theta$, which falls into the closed range $[-1, 1]$. Therefore, given a nominal value and deviation, we can convert the uncertain variable into a function that varies by a scale factor. We also impose a budget-based uncertainty set into the constraints within each time period θ, as follows.

$$\mathcal{U} = \left\{ \xi_\theta : |\xi_\theta| \leq 1, \sum_{\tau=1}^{\theta} \xi_\theta \leq \Gamma_\theta, \forall \theta \in \Theta \right\}$$

With the predefined budget, we can avoid large deviations caused by many cumulative demands, and obtain a reasonable worst-case" solution. Herein, the main assumption is that the deviation increases with the number of periods θ considered, but the cumulative value should not exceed budget Γ_θ. Thus, we can control the degree of the conservativeness of the robust solution by varying the budget of uncertainty. Consequently, we obtain a reasonable trade-off between optimality and robustness.

3.3.2. Step 2: Formulate the robust counterpart model

According to the definition of the RO theory, we formulate the robust counterpart model with a specified uncertainty set. First, to determine the RC for each related inequality, we replace d_θ with $d_\theta = \bar{d}_\theta + \xi_\theta \hat{d}_\theta$ in the AO2D model (13). Moreover, the guarantee that any solution is "immunized" against all realizations of the uncertain demand must hold true for all ξ over the budget-uncertainty set. Thus, we reformulate the inequality constraints in the AO2D model as follows.

$$GV_0 + \sum_{\tau=1}^{\theta} \left(\omega_\tau - \left[\bar{d}_\tau (\rho, z) + \xi_\theta \hat{d}_\tau (\rho, z) \right] - u_\tau(\delta, \epsilon) \right) \leq v_\theta, \quad \forall \theta \in \Theta, \xi \in \mathcal{U} \tag{14}$$

Based on the abstract distribution model AO2D (13), we first formulate a TSRO model under the worst case, as follows.

$$(\text{TSRO}) \begin{cases} \max\limits_{\omega,\rho,z} \quad f_1(\omega) - \min\limits_{\xi \in \mathcal{U}} \{\Phi(\delta, \epsilon, \xi)\} \\ \Phi(\xi) = \min\limits_{\delta,\epsilon} \quad f_2(\delta) + f_3(\epsilon) \\ s.t. \sum\limits_{\tau=1}^{\theta} \left(u_\tau(\delta, \epsilon) + \hat{d}_\tau(\rho, z)\, \xi_\tau \right) \geq GV_0 + \sum\limits_{\tau=1}^{\theta} \left(\omega_\tau - \bar{d}_\tau(\rho, z) \right) - v_\theta \\ \quad \forall \theta \in \Theta, \xi \in \mathcal{U} \end{cases} \tag{15}$$

where $\omega, \delta, \epsilon, \rho, z$ are decision variables and are as the same as model AO2D.

3.3.3. Step 3: Reformulate the tractable model

The above formulation of the TSRO is recast via duality, which is suitable for directly using off-the-shelf optimizers, such as CPLEX, GUROBI, and SCIP. For brevity, we show the reformulation procedure for the uncertainty constraint (14) according to its worst-case reformulation, which corresponds to maximizing its left-hand side over the uncertainty set as $\mathcal{U}$. For the $(i, \theta)^{th}$ pair of uncertain constraints, the worst-case reformulation is

$$\sum_{\tau=1}^{\theta} \left(\omega_\tau - \bar{d}_\tau(\rho, z) - u_\tau(\delta, \epsilon) \right) + \Delta_\theta(\xi) \leq v_\theta \tag{16}$$

Given a fixed vector of pair (ρ, z), the inequality (16) amounts to solving the two auxiliary linear programming problems:

$$\Delta_\theta(\xi) = \begin{cases} \max \quad \sum\limits_{\tau=1}^{\theta} \hat{d}_\tau(\rho, z) \xi_\tau \\ s.t. \quad \sum\limits_{\tau}^{\theta} \xi_\tau \leqslant \Gamma_\theta \quad \forall \theta \\ \quad -1 \leqslant \xi_\theta \leqslant 1, \quad \forall \theta \end{cases} \tag{17}$$

Because the auxiliary linear programming problem (17) is feasible and bounded by strong duality, the optimal objective of this problem is equal to the optimal objective of its duality. By reinjecting the duality of the auxiliary problem (17) in the TSRO (15), we obtain the following tractable optimization problem (18); herein, constraint (i) imposes a set of protective variables, and constraints (ii-iii) restrict the dual variables.

$$
(\text{TSRO}) \begin{cases} \min\limits_{\omega,\rho,y,\delta,\epsilon\in\mathcal{D}} \quad f_1(\omega) - f_2(\delta) - f_3(\epsilon) & \\ s.t. \sum\limits_{\tau=1}^{\theta} \left(\omega_\tau - \bar{d}_\tau(\rho,z) - u_\tau(\delta,\epsilon)\right) + \beta_\theta \Gamma_\theta + \sum\limits_{\tau=1}^{\theta} \alpha_{\theta,\tau} \le v_\theta \quad \forall \tau,\theta & \text{(i)} \\ \qquad \beta_\theta + \alpha_{\tau,\theta} \ge \hat{d}_\tau(\rho,z) \qquad \forall \theta, \tau \le \theta & \text{(ii)} \\ \qquad \alpha_{\tau,\theta} \ge 0, \beta_\theta \ge 0 \qquad \forall \theta, \tau \le \theta & \text{(iii)} \end{cases} \tag{18}
$$

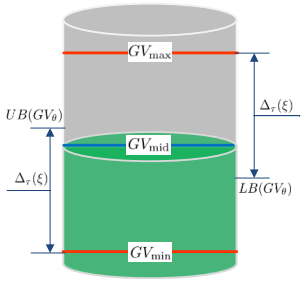

Fig. 5: Upper and lower bound of gasholder level

From Eqs. (8) and (16), we can deduce the upper and lower bound of gasholder level, as $\text{UB}(GV_\theta) = GV_{\max} - \Delta_\theta(\xi), \text{LB}(GV_\theta) = GV_{\min} + \Delta_\theta(\xi)$. If $\text{UB}(GV_\theta) < \text{LB}(GV_\theta)$, the TSRO (18) is supposed to be infeasible, as shown in Fig. 5. To keep $\text{UB}(GV_\theta) \ge \text{LB}(GV_\theta)$, we must let $\Delta_\theta(\xi) \le (GV_{\max} - GV_{\min})/2$. Therefore, we need to bound Γ_θ when implementing the TSRO in practice.

4. Interval demands forecasting for continuous processes

Because the oxygen is consumed smoothly in the continuous processes, we assume that the nominal demand and its maximum deviation in each period are equal. In this section, we parameterize the total oxygen demand of user q during each period as λ_t for brevity, $t \in T$, and develop a time-series model to forecast the oxygen demand of the next distribution horizon.

4.1. Time-series forecasting

According to the first principle of the ironmaking process, the goal of a forecasting model is to determine a function $\phi(\cdot)$ based on potential exogenous inputs, such as material (ore and coke components) and operational conditions (temperature of flame and blast air). Because first-principle forecasting models are too complex and highly time-consuming, they cannot be directly applied in the EMS. To provide an accurate and efficient forecast, we ignored the exogenous inputs of the ironmaking process and identified oxygen consumption as a time-varying output because it is smooth and continuous under normal conditions.

Typically, a time series tends to exhibit high correlations induced by the temporal structure of the data. Let us consider a time series of oxygen demand, λ_t. Let the state $y_t = [\lambda_{t-1}, \ldots, \lambda_{t-TL}]^T$, the time series forecasting model is defined as follows [35].

$$
\lambda_t = \phi(y_t) + \varepsilon_t = \phi(\lambda_{t-1}, \ldots, \lambda_{t-TL}) + \varepsilon_t \tag{19}
$$

where TL represents the size of a time lag (the number of past values), t indicates the horizon in the past, and ε_t is a white noise follows Gaussian distribution. Next, we assume that a training input $\mathbf{y} = (y_{t-1}, \ldots, y_{t-n})$

with a size of n is obtained. Because a Gaussian process (GP) (refer to [36] for details) exhibits significant advantages on quantifying uncertainty, we employ it for modeling a time-series forecasting function $\phi(\cdot)$ in this study.

4.2. GP-based time-series model

For selected time horizons $t_1, t_2, \ldots, t_i, \ldots, t_n$, GP is a stochastic process of $\phi(y_t)$, where the probability distribution is $\mathcal{P}\left[\phi(y_{t_1}), \ldots, \phi(y_{t_n})\right]$ is a multivariate Gaussian. To formulate a GP model, we first define a mean function $\mu(y_{t_i}) = \mathbb{E}\left[\phi(y_{t_i})\right]$ and a covariance function (which is also referred to as a kernel function) $k\left(y_{t_i}, y_{t_{i'}}\right) = \mathrm{Cov}\left[\phi(y_{t_i}), \phi(y_{t_{i'}})\right] = \mathbb{E}\left[(\phi(y_{t_i}) - \mu(y_{t_i}))(\phi(y_{t_{i'}}) - \mu(y_{t_{i'}}))\right]$. Note, that the covariance between the outputs is written as a function of the inputs. Thus, the specification of the kernel function implies the shape of the distribution over functions.

For the training set $\mathbf{y} = \{y_{t_1}, y_{t_2}, \cdots, y_{t_n}\}$, we can define the following covariance matrices.

$$\mathcal{K}(\mathbf{y}, \mathbf{y}) = \begin{bmatrix} k(y_{t-1}, y_{t-1}) & \cdots & k(y_{t-1}, y_{t-N}) \\ \vdots & \ddots & \vdots \\ k(y_{t-N}, y_{t-1}) & \cdots & k(y_{t-N}, y_{t-N}) \end{bmatrix} \tag{20}$$

We then denote the prior distribution of λ by

$$\lambda \sim \mathcal{N}\left(\mu(\mathbf{y}), \mathcal{K}(\mathbf{y}, \mathbf{y}) + \sigma_n^2 \mathbb{I}\right) \tag{21}$$

Our main concern is get the posterior distribution over functions $\mathcal{P}\left(\lambda_t \mid \mathbf{y}, \boldsymbol{\lambda}, y_t\right)$ based on the training data. First, we define the new joint distribution between training target λ and undergoing function $\phi(\cdot)$.

$$\mathcal{P}\left(\begin{bmatrix} \mathbf{y} \\ \phi(y_t) \end{bmatrix}\right) = \mathcal{N}\left(\begin{bmatrix} \boldsymbol{\mu}(\mathbf{y}) \\ \mu(y_t) \end{bmatrix}, \begin{bmatrix} \mathcal{K}(\mathbf{y}, \mathbf{y}) + \sigma_n^2 \mathbb{I} & \mathcal{K}(\mathbf{y}, y_t) \\ \mathcal{K}(y_t, \mathbf{y}) & k(y_t, y_t) \end{bmatrix}\right) \tag{22}$$

where

$$\mathcal{K}(y_t, \mathbf{y}) = [k(y_t, y_{t-1}), \cdots, k(y_t, y_{t-N})] \tag{23}$$

After some manipulations of the joint Gaussian distribution, the resulting posterior distribution over $\phi(y_t)$ is also a GP with the mean $\hat{\mu}_t$ and variance $\hat{\sigma}_t^2$, which are defined as follows.

$$\hat{\mu}_t = \mathcal{K}(y_t, \mathbf{y})\left[\mathcal{K}(\mathbf{y}, \mathbf{y}) + \sigma_n^2 \mathbb{I}\right]^{-1}\left[\lambda - \mu(\mathbf{y})\right] + \mu(y_t) \tag{24}$$

$$\hat{\sigma}_t^2 = k(y_t, y_t) - \mathcal{K}(y_t, \mathbf{y})\,\mathcal{K}\left[\mathcal{K}(\mathbf{y}, \mathbf{y}) + \sigma_n^2 \mathbb{I}\right]^{-1}\mathcal{K}(\boldsymbol{y}, y_t) \tag{25}$$

Next we can infer that the the mean of λ_t, $\mu(\lambda_t) = \hat{\mu}_t$, the variance of λ_t, $\sigma^2(\lambda_t) = \hat{\sigma}_t^2 + \sigma_n^2 \mathbb{I}$. Because the correlation between any pair of forecasting λ_t is specified by the covariance functions, we combine and modify the existing functions [36] to model the shape of the set of observations and predictions. The forecasting model works as follows: it predicts only one time horizon ahead, using the estimate of the output of the current time, as well as previous outputs (up to the lag TL), as the input to the prediction of the next time step (for more details, refer to [35]). Via the GP-based forecasting model, we can quantify the uncertainty of λ_t and get the nominal and deviation values of the oxygen demand in each period (as shown in Fig. 6).

5. Multi-scenario demands for discrete processes

Because the oxygen demand shape of a discrete process $d_{q,\theta}$ is non-smooth, we cannot directly calculate the nominal demand and its maximum deviation during each period. However, they are directly linked to the schedule of the steel plant. In this section, we propose a scheduling model for the EMS to generate multiple scheduling solutions by defining different capacity limits.

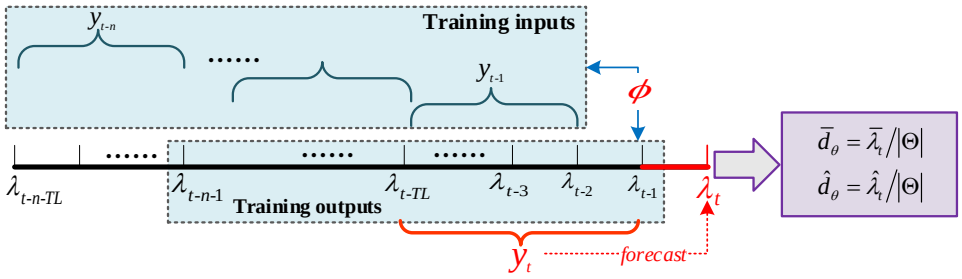

Fig. 6: Forecast demand by GP-base time series

5.1. Scheduling for steelmaking production

Scheduling in a steel plant is linked to a set of stages ($G = 1, \cdots, g, \cdots, |G|$), through which high-temperature molten iron from ironmaking processes is converted into solidified slabs. Scheduling focuses on sequencing a job set $J = 1, \cdots, j, \cdots, |J|$ that has some tasks $A_{g,j}$ in its routing, allocating an eligible machine for each task, and optimizing certain criteria, such as makespan and waiting time. The task set of each job must follow the same order from the steelmaking to the casting stage. In the casting stage, the tasks must be performed in batches, without interruptions, because the liquid steel is solidified continuously within a period. Considering such procedural, temporal, and resource constraints, the scheduling model of the steelmaking processes is always identified as a variant of the hybrid flow shop-scheduling problem [38].

Given a fixed schedule, we can calculate the oxygen demands in period θ via its process units ($PT^{\theta}_{g,j}$) allocated in period θ (as shown in Fig. 7). Next, we can estimate the nominal value and deviation of uncertain energy demand using the GP-based approach from our previous study [37]. To reduce the effect on the oxygen distribution system, the demand shape needs to be shifted through peak clipping and valley filling. Because the number of simultaneous processing tasks (referred to as capacity) directly determines the oxygen consumption, we propose a capacity-constrained shifting method to adjust the oxygen on the demand side.

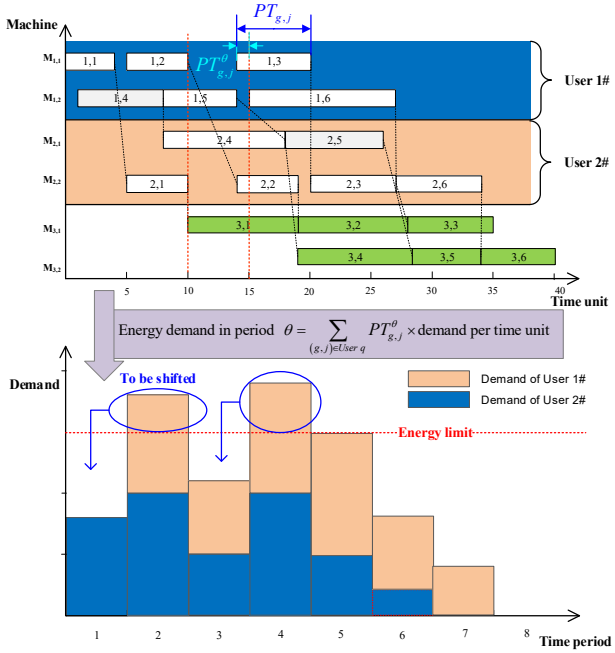

Fig. 7: A Gantt chart for the feasible schedule executed in a steel plant

5.2. Preprocessing procedure

Depending on the problem size and complexity, scheduling methodologies, involving resource constraints, can be divided into two groups: monolithic and sequential [39]. Monolithic approaches simultaneously solve the job assignment, sequencing problem, and timing problems. In contrast, sequential approaches assume that the job sequencing and machine allocation problems have already been solved. Considering the advantage of computational complexity, we adopt a sequential approach and represent the solution of the job sequencing and machine allocation with a directed graph $\mathcal{G}$ (Fig. 8), where $(0, 0)$ is a dummy task.

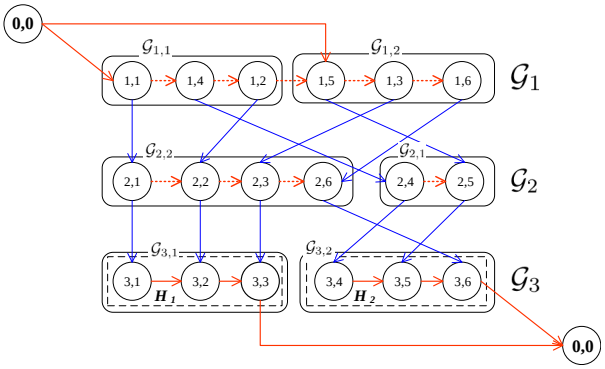

Fig. 8: A directed graph $\mathcal{G}$ for a schedule released into a steel plant

Because the timing optimization problem is highly sensitive to the number of time-indexed variables and constraints, we perform a preprocessing procedure on the directed graph and compute the earliest starting times ($ES_{g,j}$) and latest finishing times ($LF_{g,j}$) for each task. Given a fixed $\mathcal{G}$, let

- $\mathcal{G}_g$ and $\mathcal{G}_{g,m}$ respectively represent tasks allocated in stage g and the m^{th} machine in M_g,
- $A_{gg,j}$ is the next task of $A_{g,j}$ and $A_{g,jj}$ is the next task of $A_{g,j}$ on the same machine

Here, the two-pass method called forward-backward scheduling (as in Algorithm 1) is used to estimate $ES_{g,j}$ and $LF_{g,j}$.

5.3. Model formulation

In this section, we develop a discrete-time MILP model for the capacity-constrained steelmaking scheduling problem. The model is based on the definition of binary variables (x_{g,j_l}) that describes the processing state of task A_{g_j} at each time unit l.

5.3.1. Objectives

Considering the productivity and energy loss, the objective of the steelmaking scheduling problem is to minimize the sum of make-span ($C_{\max}$) and waiting times (W_{tot}).

$$\begin{aligned} \min F &= C_{\max} + W_{\text{tot}} \\ &= \max_{j \in J} C_{|G|,j} + \sum_{j \in J} \left(C_{|G|,j} - C_{1,j} - \sum_{g=1}^{|G|-1} PT_{g,j} \right) \end{aligned} \tag{26}$$

5.3.2. Constraints

A feasible schedule executed in a steel plant must satisfy the following constraints.

(1) Each task can only start at exactly one time unit.

$$\sum_{l=1}^{|L|-PT_{g,j}+1} x_{g,j,l} = 1, \quad \forall g \in G, j \in J \tag{27}$$

Algorithm 1: Forward-backward scheduling

Input: Directed graph $\mathcal{G}$

Output: Earliest starting Time($ES_{i,j}$) , Latest finish times($LF_{i,j}$)

/*Notes: $\bar{S}_{g,j}$ $\bar{C}_{g,j}$ represent estimated starting and finishing time of $A_{g,j}$ */

/*Step 1. forward scheduling*/

Set $\bar{S}_{0,0} := 0$;

for $gg = 1$ *to* $|G|$ **do**

  foreach $A_{gg,jj} \in \mathcal{G}_{gg}$ **do**

    $\bar{S}_{gg,jj} := \bar{S}_{gg,j} + PT_{gg,j} + 1$;

  foreach $A_{gg,j} \in \mathcal{G}_{gg}$ **do**

    $ES_{gg,j} := \max\left\{\bar{S}_{g,j} + PT_{g,j} + TT_{g,gg} + 1, \bar{S}_{gg,j}\right\}$;

    $\bar{S}_{gg,j} := ES_{gg,j}$;

/*Step 2. backward scheduling*/

$\bar{S}_{0,0} = T$

for $g = |G| - 1$ *to* 1 **do**

  foreach $A_{g,j} \in \mathcal{G}_g$ **do**

    $\bar{C}_{g,j} = \bar{C}_{g,jj} - PT_{g,jj} - 1$;

  foreach $A_{g,j} \in \mathcal{G}_g$ **do**

    $LF_{g,j} := \max\left\{\bar{C}_{gg,j} - PT_{gg,j} - TT_{g,gg} - 1, \bar{C}_{g,j}\right\}$;

    $\bar{C}_{g,j} := LF_{g,j}$;

(2) The completion time of task $A_{g,j}$ can be defined as

$$C_{g,j} = \sum_{l=1}^{|L|-PT_{g,j}+1} (l-1)\, x_{g,j,l} + PT_{g,j}, \quad \forall g \in G, j \in J \tag{28}$$

(3) For every two connected tasks of the same job (i.e., $A_{g,j}$ and $A_{gg,j}$), the next task ($A_{gg,j}$) cannot be started unless the previous one ($A_{g,j}$) has been completed and delivered.

$$C_{gg,j} - C_{g,j} \geq PT_{g,j} + TT_{g,gg} + 1, \quad \forall g, gg \in G, j \in J \tag{29}$$

(4) For every two connected tasks on the same machine (i.e., $A_{g,j}$ and $A_{g,jj}$), the next task ($A_{g,jj}$) cannot be started unless the previous one $A_{g,j}$) has been completed.

$$C_{g,jj} - C_{g,j} \geq PT_{g,jj} + 1, \quad \forall g \in G, j, jj \in J \tag{30}$$

(5) The number of jobs simultaneously processed at time t cannot be greater than the total number of available resources. Here, $\mathcal{A}^O$ represents the stages consuming oxygen $WL_s^{\max}$ represents the capacity limitation under scenario s.

$$\sum_{A_{g,j} \in \mathcal{A}^O} x_{g,j,l} \leq WL_s^{\max}, \quad \forall l \in [ES_{g,j}, LF_{g,j}] \tag{31}$$

(6) A minimum setup time at the casting stage must be guaranteed before the first job of a new batch (hh) starts.

$$C_{|G|,firstOf(hh)} - C_{|G|,lastOf(h)} = PT_{|G|,firstOf(hh)} + SU_{hh}, \quad \forall h, hh \in H \tag{32}$$

where $firstOf(\cdot)$ and $lastOf(\cdot)$ denote the first and last job in a batch, respectively.

(7) The processing precedence constraints of jobs in the same batch in the last stage are as follows:

$$C_{|G|,jj} - C_{|G|,j} = PT_{|G|,jj} + 1, \quad \forall h \in H \wedge j, jj \in J(h) \tag{33}$$

According to the above formulation (Eq. 26 - 33), it is worth noting that the scheduling model link to the optimal oxygen distribution model only via capacity limit $WL_s^{\max}$ and constraint (31). Therefore, the value of z_s in TPSO will impact the objective of the scheduling model.

6. Computational studies

In this section, we present the computational studies that verify our proposed models with the flowchart shown in Fig. 9, and test their ability to effectively distribute oxygen under uncertainty as the following steps.

(1) Test the GP-based time series model, which predict oxygen demands of each ironmaking process q within current distribution horizon t, and estimate the point and interval demands $(\bar{d}_{q,\theta}, \hat{d}_{q,\theta})$ of each time period.

(2) Test the multi-scenario process scheduling model, which generate oxygen demands $(d^s_{q,\theta})$ via under different capacity limits $(WL_s^{\max})$ in steel plants.

(3) Analyzed the proposed TSRO model for oxygen distribution under uncertainty including its budget levels, sensitivity and robustness.

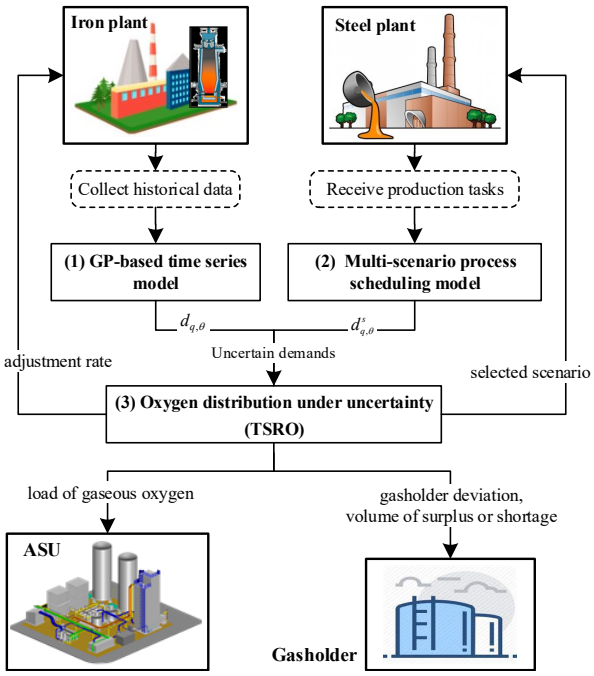

Fig. 9: Interactions between TSRO, forecasting and scheduling

The TSRO and scheduling model were programmed in Pyomo [40], which is a Python-based, open-source algebraic modeling language, and solved by "Gurobi 9.0" (`https://www.gurobi.com/products/gurobi-optimizer/`, an academic version with default settings), which is a state-of-the-art optimizer for mathematical programming. For GP implementation, we adapted the open-source scikit-learn package, version 0.24.1 [41]. All computational studies were executed on a PC with an Intel Core i7 processor (3.60 GHz), 16 GB RAM, and Windows 10 operating system.

Case studies addressed in this section were performed by applying our methods in an integrated iron and steel plant in China, which has two ASUs in OGS, five oxygen users in OUS including two ironmaking processes, two steelmaking processes and a small user from other processes. In the following studies, we collected statistical data on manufacturing and energy from the EMS, and randomly synthesized energy

distribution instances with different demand levels. All testing instances have been shared on GitHub (`https://github.com/janason/Energy/tree/master/02`).

6.1. Interval demands forecasting via GP

To validate the forecasting model, we collected actual daily oxygen data for three months (90 days); three horizons were collected each day: $90 \times 3 = 270$ samples in total. We used 235 samples for training and 35 samples for testing the oxygen demand with one horizon ahead. The GP-based time-series model was implemented using scikit-learn's class *GaussianProcessRegressor*. We specified the prior mean to be *zero* and prior covariance by passing a mixture *kernel* object with a squared exponential and white noise covariance function. We ran the forecasting model with 10 random restarts, with a maximum of 2,000 iterations, and evaluated it with metrics known as mean absolute percentage error (MAPE) and prediction interval normalized average width (PINAW)

$$MAPE = \frac{1}{N} \sum_{t \in T'} \left| \frac{\bar{\lambda}_t - \lambda_t}{\lambda_t} \right| \times 100\%$$

$$PINAW = \frac{1}{N \left(\max\limits_{t \in T'} \lambda_t - \min\limits_{t \in T'} \lambda_t \right)} \sum_{t \in T'} (U_t - L_t)$$

where T' is time horizons in testing set with the size of N, λ_t and $\bar{\lambda}_t$ represent the actual and predicted value, U_t and L_t denote the lower bound and upper bound of 95% confidence intervals. MAPE is used for evaluating the accuracy of prediction values, while PINAW is used for further evaluating the quality of prediction intervals.

The testing results of the studied processes listed in Table 1. To investigate the forecasting performance in a more intuitive manner, we graphically illustrated the probabilistic forecasting results in Fig. 10 which plots the observed and forecasted oxygen demands, and represents their predictions intervals with shaded boundaries. According to the results, the forecasting model with time lag $TL = 5$ is better than the one with time lag $TL = 1$, because the former one has smaller MAPE values and greater PINAW values. The figures also confirm the results, where $TL = 5$ plots curves more closed to actual values, and has more narrow intervals. Therefore, it is beneficial to reduce conservativeness of TSRO model.

Table 1: evaluation indices on ironmaking processes

Data set	MAPE		PINAW	
	TL=1	TL=5	TL=1	TL=5
ironmaking process 1#	5.60%	2.70%	1.15	0.73
ironmaking process 2#	4.60%	2.50%	1.08	0.69

6.2. Multi-scenario demands via capacity-constrained scheduling

As previously mentioned, multiple scenarios exist for steelmaking production scheduling, and each of them has different demands for oxygen. The investigated iron and steel plant has two steelmaking processes as two independent energy users. In the first process, two machines are used for dephosphorization. In the second process, three machines are used for decarbonization. In this study, we selected three representative scheduling instances and generate their multi-scenario energy demands by setting the two capacity limits for the steelmaking processes.

- Scenario 1: The maximum capacity $WL_1^{\max} = 5$, where the number of simultaneous processing tasks is not greater than 5.

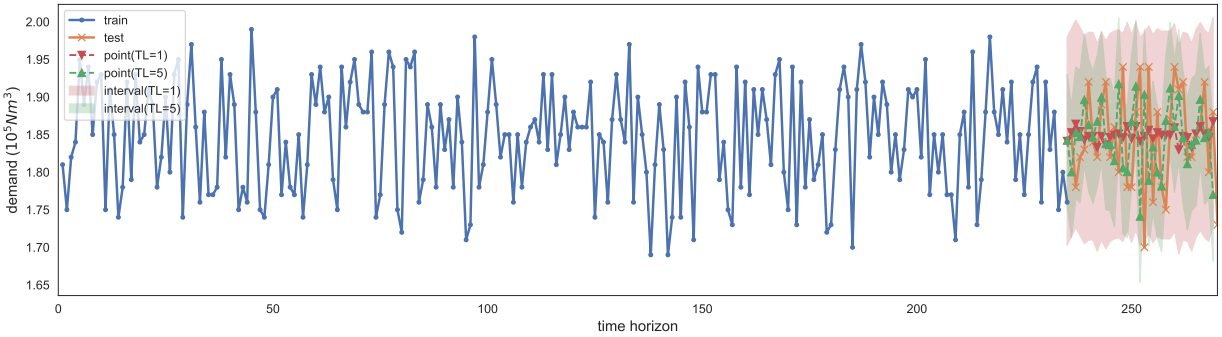

(a) ironmaking process 1#

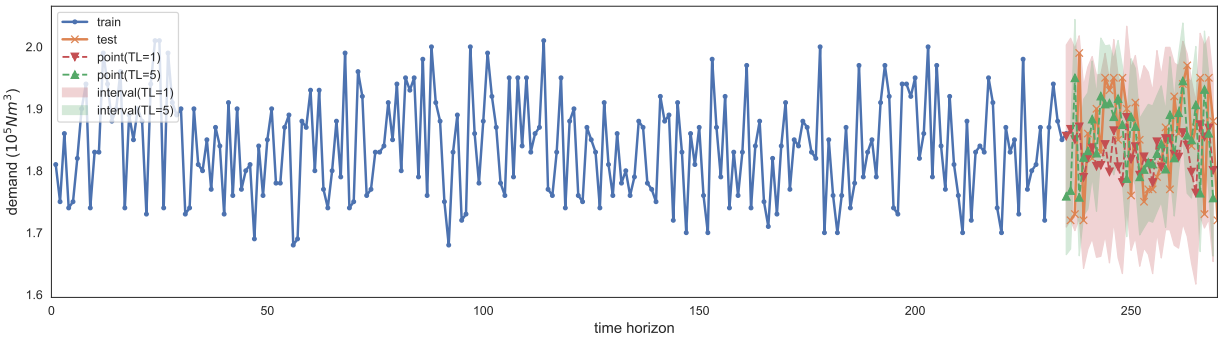

(b) ironmaking process 2#

Fig. 10: Probabilistic forecasts of oxygen interval demand

- Scenario 2: The maximum capacity $WL_2^{\max} = 4$, where the number of simultaneous processing tasks is not greater than 4.

The scheduling results under each scenario are represented with Gantt charts (Fig. A1-Fig. A3). Based on scheduling results and statistics in EMS, we plotted the demand curves (Fig. B1-Fig. B3) of each user for 32 periods, spanning 15 min each. Because the steelmaking process is the bottleneck of the steel plant when its capacity limit becomes smaller, there are not sufficient machine resources to process tasks. Thus the starting times of the next stages are likely to be delayed. Observed the scheduling objectives shown in Fig. 11, the optimal scheduling objectives ($C_{\max}$ and W_{tot}) deteriorate when the capacity is constrained. The statistics results of oxygen demand in each period are plotted in Fig. 12. When the capacity limit is lower, there are fewer tasks to require for energy simultaneously. Therefore, the mean demands under scenario 2 are lower than scenario 1. The demand variations under scenario 2 are also lower than scenario 1. This is because the idle time of each machine is reduced, which also make the waiting time objective (W_{tot}) increase. In other words, the multi-scenario scheduling model can provide demands with multiple shapes for the TSRO and contributes to flexibility for oxygen distribution.

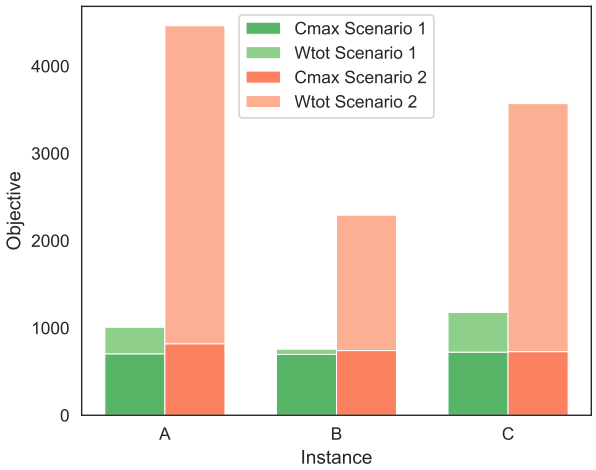

Fig. 11: Scheduling objective of each instance

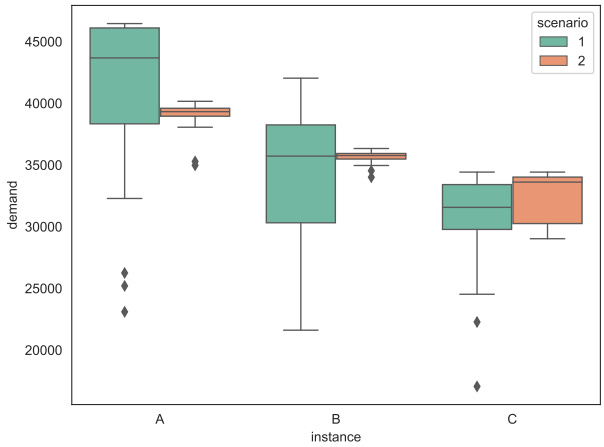

Fig. 12: Energy demand of each instance

6.3. Analysis of TSRO model

To analyze the performance of the TSRO model, we extracted the following model parameters from the EMS database.

- Load of each ASU: $\omega_r^{\min} = 1.5 \times 10^4 \mathrm{Nm}^3, \omega_{\mathrm{r}}^{\max} = 2.0 \times 10^4 \mathrm{Nm}^3$.
- Maximum ramp: $\hat{\omega}^{\max} = 300 \mathrm{Nm}^3$.
- Adjustment rate of continuous users: $\rho_q^{\min} = 0.8, \rho_q^{\max} = 1.2$.
- Scheduling scenario of discrete users: $S = \{1, 2\}$
- Total capacity of OSS: $GV = 6 \times 10^4 \mathrm{Nm}^3$.
- Initial volume of OSS: $GV_{\min} = 0.1GV, GV_{\max} = 0.9GV$, $GV_{\mathrm{mid}} = 0.5GV$
- Objective coefficients: $\gamma_1 = 1.0, \gamma_2 = 2.0, \gamma_3 = 20.0$
- Number of the time period: $|\Theta| = 32$.

In the following studies, we assume that the estimated oxygen demand of each user (as shown in Fig. B1-Fig. B3 in the Appendix) is randomly varied between $[\bar{d}_\theta - \hat{d}_\theta, \bar{d}_\theta + \hat{d}_\theta]$ and $\hat{d}_\theta = \eta \times \bar{d}_\theta$. Here, η has two candidate levels ($\eta_1 = 0.05$ and $\eta_2 = 0.08$) that cover 68% and 90% confidence intervals, respectively.

6.3.1. Choice of budget levels

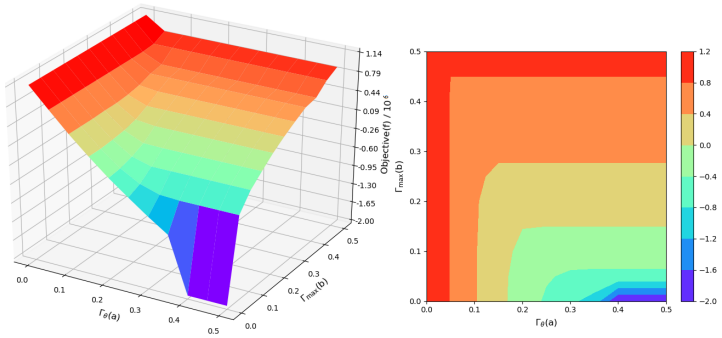

(a) $\eta = 0.05$, critical point $(a = 0.05, b = 0.40)$

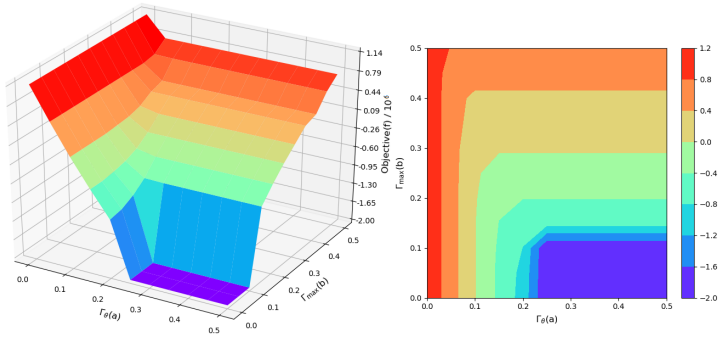

(b) $\eta = 0.08$, critical point $(a = 0.10, b = 0.25)$

Fig. 13: Response under different budget levels

As discussed in Section 3.3, we introduced budget parameters Γ_θ and $\Gamma_{\max}$ in the TSRO to control the trade-off between the probability of constraint violation and the optimality of the objective function. We define the time-varying budget, as follows.

$$\Gamma_\theta = \min\left\{Z_{1-a}\sqrt{\theta} + 1, b\,|\Theta|\right\},$$

where a denotes the risk level, Z is the quantile of the standard normal distribution, and b is a constant coefficient. The first term is used to control robustness, and the second term is set for the upper bound of Γ_θ to maintain feasibility.

To choose an appropriate combination of (a, b), we adopted instance B as the test representative, and selected a and b from $[0, 0.5]$ with step 0.05. Hence, we obtained $11 \times 11 = 121$ candidate budgets. Subsequently, we ran the TSRO with different values of (a, b), and plotted the response surfaces of two deviations ($\eta_1 = 0.05$ and $\eta_2 = 0.08$), as shown in Fig. 13. If the TSRO is infeasible, let $f = -2.0 \times 10^6$. These results demonstrate that the objective value of f increases as the risk level decreases or as the maximum budget decreases. When $a \geq 0.05$ or $b \leq 0.40$, solutions with a deviation of 0.05 are feasible. When $a \geq 0.10$ or $b \leq 0.25$, solutions with a deviation of 0.08 are feasible. According to these critical points in the figures, we recommend $a = 0.10$ and $b = 0.40$ in the subsequent computational studies.

6.3.2. Sensitivity analysis of ramp capacity

In this section, we study the relationship between the ramp capacity of the ASU and the performance of the robust models. The assumption is that a higher ramp capacity improves the ability of the EMS to address a high variation in oxygen. Therefore, we aimed to verify the advantages of the TSRO model under different ramp capacities between $[0, 500]\,Nm^3$ with steps of $50Nm^3$.

Fig. 14 summarizes the computational results for two group studies: the deviation levels of $\eta_1 = 0.05$ and $\eta_2 = 0.08$. The results indicate that the TSRO models for instances A and C can obtain more optimal objectives by enlarging the ramping capacity when the ramping capacity $\hat{\omega}_{\max} \leq 200$; however, the model for instance B retains its optimal objective. This clearly demonstrates that models with higher and lower demands require a design of an appropriate ramp capacity to improve their profits.

6.3.3. Robustness comparison by simulation

With the budget-based uncertainty set $\mathcal{U}$, the TSRO model provides a protective solution. We randomly sampled two demand vectors d_θ^1 and d_θ^2, following a truncated normal distribution between $\left[\bar{d}_\theta - \hat{d}_\theta, \bar{d}_\theta + \hat{d}_\theta\right]$. Let the random demand sample $d_\theta = (d_\theta^1 + d_\theta^2)/2$. The random sample may be located outside the budget-based uncertainty set. Thus, we can test the robustness of the proposed TSRO model. In the following studies, we tested three instances (A-C) with five different initial gasholder levels (GV_0 is between 0.3 and 0.7 GV); hence, we obtained $3 \times 5 = 15$ cases under each deviation ($\eta \in \{0.05, 0.08\}$). Next, we independently ran the distribution model with deterministic optimization (DO) [12] and the proposed TSRO with a fixed budget level ($a = 0.10, b = 0.40$). We also scholastically simulated the solutions of DO and TSRO with 1,000 rounds (-simulated).

Fig. 15 shows the objective values of DO and RO and their average objectives under simulation with 95% confidence intervals (two standard deviations). The results indicate that the objective of the TSRO is lower than that of the DO; however, the objective of the TSRO provides promising protection that is lower than the 95% confidence intervals. Under stochastic environments, the simulated objective of the TSRO is only slightly lower than that of the simulated DO, indicating that the objective of the TSRO is less conservative. Unsurprisingly, the DO fails to hedge against uncertainty for most instances, except in some cases with instance B (with medium demand). Because a too large or small demand can increase the risk of an imbalance of oxygen distribution, we must reduce demand fluctuation when implementing the distribution model in practice.

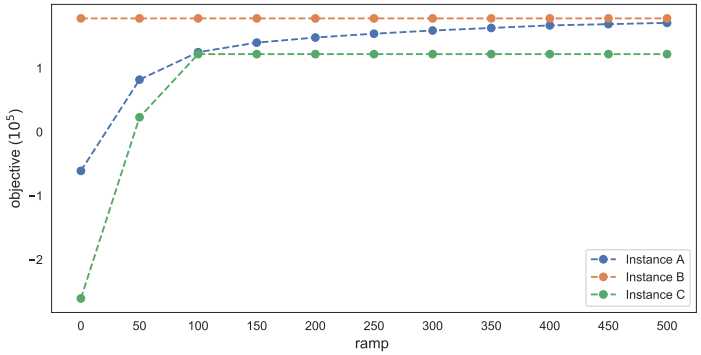

(a) $\eta_1 = 0.05$

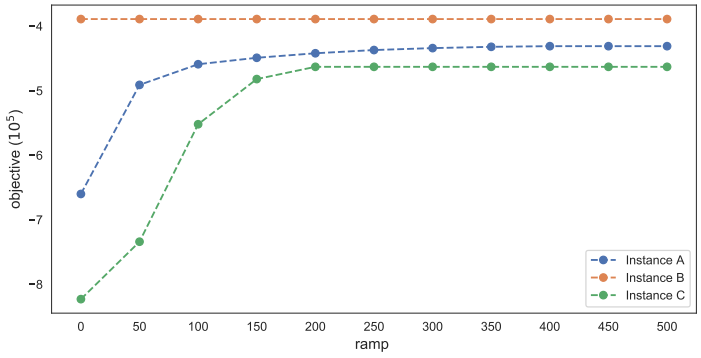

(b) $\eta_2 = 0.08$

Fig. 14: Response under different ramp capacities

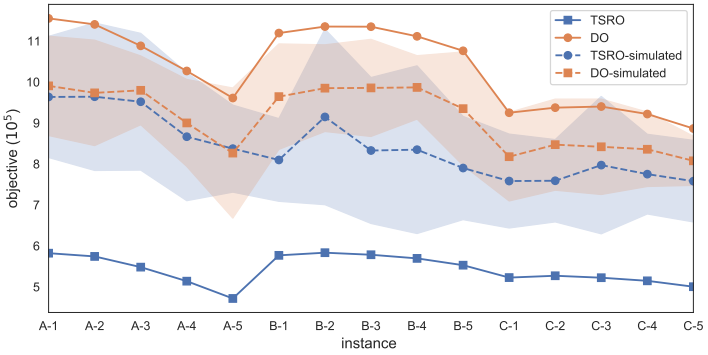

(a) $\eta_1 = 0.05$

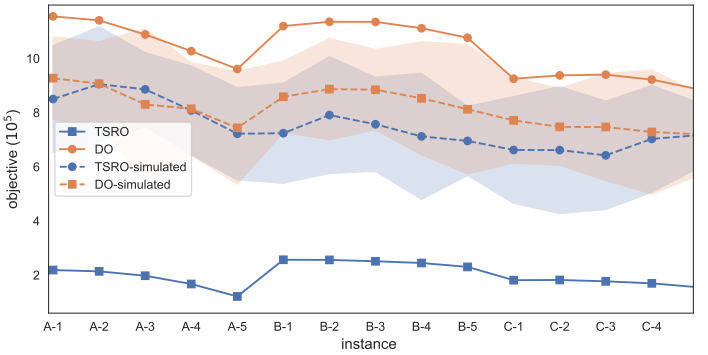

(b) $\eta_2 = 0.08$

Fig. 15: Simulation results of different cases

7. Conclusions

In this study, we investigated the problem of optimal oxygen distribution with flexible demands under uncertainty. We proposed a TSRO model with a budget-based uncertainty set that protected the initial distribution policy with low conservatism. The following conclusions were drawn based on computational studies.

(1) The GP-based time-series model can forecast varied oxygen demands with 95% confidence intervals. The capacity-constrained rescheduling model can effectively shift step-wise oxygen demands.
(2) According to the level of risk aversion, the decision-maker can select appropriate budget parameters for the TSRO model. The ramp capacity also contributed to the flexibility of the oxygen distribution.
(3) In contrast to the DO commonly used in existing studies, the TSRO model can provide a safer solution; however, its average performance has not deteriorated under uncertainty.

In conclusion, the model simulation is consistent with our design and confirms that the proposed model provides a promising solution for the uncertain oxygen distribution problem. In the future, the following problems need to be studied further.

(1) In the investigated problem, we only considered uncertain energy demands from the manufacturing system. However, several other uncertain factors, such as energy market demands and machine breakdowns, should be investigated.
(2) In the proposed TSRO model, we only know the interval of the uncertain demands; however, the probabilistic information was not embedded in the model. Therefore, building a data-driven uncertainty set should be considered.

Acknowledgment

This research was financially supported by the by the National Natural Science Foundation of China under Grant 61873042 and 51734004, in part by the Open Fund of Guangxi Key Laboratory of Automatic Detection Technology and Instrument (No. YQ19202). Thanks to the China Scholarship Council (CSC) for supporting a 1-year visit at University College London (UCL), U.K.

References

[1] Maria T Johansson. Effects on global co 2 emissions when substituting lpg with bio-sng as fuel in steel industry reheating furnaces—the impact of different perspectives on co 2 assessment. *Energy efficiency*, 9(6):1437–1445, 2016.
[2] Wenqiang Sun, Qiang Wang, Yue Zhou, and Jianzhong Wu. Material and energy flows of the iron and steel industry: Status quo, challenges and perspectives. *Applied Energy*, 268:114946, 2020.
[3] Shuaiyin Ma, Yingfeng Zhang, Jingxiang Lv, Haidong Yang, and Jianzhong Wu. Energy-cyber-physical system enabled management for energy-intensive manufacturing industries. *Journal of Cleaner Production*, 226:892–903, 2019.
[4] Wenqiang Sun, Qiang Wang, Zhong Zheng, and Jiuju Cai. Material-energy-emission nexus in the integrated iron and steel industry. *Energy Conversion and Management*, 213:112828, 2020.
[5] Dara O'Rourke. The science of sustainable supply chains. *Science*, 344(6188):1124–1127, 2014.
[6] Lennart Merkert, Iiro Harjunkoski, Alf Isaksson, Simo Säynevirta, Antti Saarela, and Guido Sand. Scheduling and energy–industrial challenges and opportunities. *Computers & Chemical Engineering*, 72:183–198, 2015.
[7] Haining Kong, Ershi Qi, Hui Li, Gang Li, and Xing Zhang. An milp model for optimization of byproduct gases in the integrated iron and steel plant. *Applied Energy*, 87(7):2156–2163, 2010.
[8] Xiancong Zhao, Hao Bai, Xin Lu, Qi Shi, and Jiehai Han. A milp model concerning the optimisation of penalty factors for the short-term distribution of byproduct gases produced in the iron and steel making process. *Applied energy*, 148:142–158, 2015.
[9] Xiancong Zhao, Hao Bai, Qi Shi, Xin Lu, and Zhihui Zhang. Optimal scheduling of a byproduct gas system in a steel plant considering time-of-use electricity pricing. *Applied Energy*, 195:100–113, 2017.
[10] Xiaoping Zhang, Jun Zhao, Wei Wang, Liqun Cong, and Weimin Feng. An optimal method for prediction and adjustment on byproduct gas holder in steel industry. *Expert Systems with Applications*, 38(4):4588–4599, 2011.
[11] Xiaolei Zhang, Yanyan Zhang, and Lixin Tang. Model of balanced distribution and optimal scheduling of the oxygen system in iron and steel industry. In *2012 IEEE International Conference on Information and Automation*, pages 61–65. IEEE, 2012.

[12] Peikun Zhang, Li Wang, and Lige Tong. Milp-based optimization of oxygen distribution system in integrated steel mills. *Computers & Chemical Engineering*, 93:175–184, 2016.
[13] Christian Gahm, Florian Denz, Martin Dirr, and Axel Tuma. Energy-efficient scheduling in manufacturing companies: A review and research framework. *European Journal of Operational Research*, 248(3):744–757, 2016.
[14] Yujiao Zeng, Xin Xiao, Jie Li, Li Sun, Christodoulos A Floudas, and Hechang Li. A novel period mixed-integer linear optimization model for optimal distribution of byproduct gases, steam and power in an iron and steel plant. *Energy*, 143:881–899, 2018.
[15] Kristian Nolde and Manfred Morari. Electrical load tracking scheduling of a steel plant. *Computers & Chemical Engineering*, 34(11):1899–1903, 2010.
[16] Pedro M Castro, Lige Sun, and Iiro Harjunkoski. Resource–task network formulations for industrial demand side management of a steel plant. *Industrial & Engineering Chemistry Research*, 52(36):13046–13058, 2013.
[17] Hubert Hadera, Iiro Harjunkoski, Guido Sand, Ignacio E Grossmann, and Sebastian Engell. Optimization of steel production scheduling with complex time-sensitive electricity cost. *Computers & Chemical Engineering*, 76:117–136, 2015.
[18] Ping Zhou, Dongwei Guo, and Tianyou Chai. Data-driven predictive control of molten iron quality in blast furnace ironmaking using multi-output ls-svr based inverse system identification. *Neurocomputing*, 308:101–110, 2018.
[19] Wenjie Xu, Lixin Tang, and Efstratios N Pistikopoulos. Modeling and solution for steelmaking scheduling with batching decisions and energy constraints. *Computers & Chemical Engineering*, 116:368–384, 2018.
[20] Han Xi, Xiao Wu, Xianhao Chen, and Peng Sha. Artificial intelligent based energy scheduling of steel mill gas utilization system towards carbon neutrality. *Applied Energy*, 295:117069, 2021.
[21] Jun Zhao, Quanli Liu, Witold Pedrycz, and Dexiang Li. Effective noise estimation-based online prediction for byproduct gas system in steel industry. *IEEE Transactions on Industrial Informatics*, 8(4):953–963, 2012.
[22] Jun Zhao, Chunyang Sheng, Wei Wang, Witold Pedrycz, and Quanli Liu. Data-based predictive optimization for byproduct gas system in steel industry. *IEEE Transactions on Automation Science and Engineering*, 14(4):1761–1770, 2016.
[23] Feng Jin, Jun Zhao, Ying Liu, Wei Wang, and Qingshan Xu. A scheduling approach with uncertainties in generation and consumption for converter gas system in steel industry. *Information Sciences*, 546:312–328, 2021.
[24] Feng Jin, Linqing Wang, Jun Zhao, Wei Wang, and Quanli Liu. Granular-causality-based byproduct energy scheduling for energy-intensive enterprise. *IEEE Transactions on Automation Science and Engineering*, 17(4):1662–1673, 2020.
[25] Zhongyang Han, Jun Zhao, Wei Wang, and Ying Liu. A two-stage method for predicting and scheduling energy in an oxygen/nitrogen system of the steel industry. *Control Engineering Practice*, 52:35–45, 2016.
[26] Zhongyang Han, Jun Zhao, and Wei Wang. An optimized oxygen system scheduling with electricity cost consideration in steel industry. *IEEE/CAA Journal of Automatica Sinica*, 4(2):216–222, 2017.
[27] Allen L Soyster. Convex programming with set-inclusive constraints and applications to inexact linear programming. *Operations research*, 21(5):1154–1157, 1973.
[28] Aharon Ben-Tal and Arkadi Nemirovski. Robust convex optimization. *Mathematics of operations research*, 23(4):769–805, 1998.
[29] Virginie Gabrel, Cécile Murat, and Aurélie Thiele. Recent advances in robust optimization: An overview. *European journal of operational research*, 235(3):471–483, 2014.
[30] Bram L Gorissen, İhsan Yanıkoğlu, and Dick den Hertog. A practical guide to robust optimization. *Omega*, 53:124–137, 2015.
[31] Dimitris Bertsimas and Melvyn Sim. The price of robustness. *Operations research*, 52(1):35–53, 2004.
[32] Haiqi Nie, Zhaoyang Li, Shibo Kuang, Lianggong Yan, Wenqi Zhong, Aibing Yu, Xiaoming Mao, and Haifa Xu. Numerical investigation of oxygen-enriched operations in blast furnace ironmaking. *Fuel*, 296:120662, 2021.
[33] Zhaojun Xu, Zhong Zheng, Xiaoqiang Gao, and Xinyue Shen. Reducing the fluctuation of oxygen demand in a steel plant through optimal production scheduling. *Journal of Cleaner Production*, 282:124529, 2021.
[34] Dimitris Bertsimas and Aurélie Thiele. A robust optimization approach to inventory theory. *Operations research*, 54(1):150–168, 2006.
[35] Agathe Girard, Carl Edward Rasmussen, Joaquin Quinonero-Candela, and Roderick Murray-Smith. Gaussian process priors with uncertain inputs-application to multiple-step ahead time series forecasting. 2003.
[36] Carl Edward Rasmussen. Gaussian processes in machine learning. In *Summer school on machine learning*, pages 63–71. Springer, 2003.
[37] Sheng-Long Jiang, Xinyue Shen, and Zhong Zheng. Gaussian process-based hybrid model for predicting oxygen consumption in the converter steelmaking process. *Processes*, 7(6):352, 2019.
[38] Yuan-yuan Tan, Ying-lei Huang, and Shi-xin Liu. Two-stage mathematical programming approach for steelmaking process scheduling under variable electricity price. *Journal of Iron and Steel Research, International*, 20(7):1–8, 2013.
[39] Pablo A Marchetti and Jaime Cerdá. A general resource-constrained scheduling framework for multistage batch facilities with sequence-dependent changeovers. *Computers & Chemical Engineering*, 33(4):871–886, 2009.
[40] William E Hart, Carl D Laird, Jean-Paul Watson, David L Woodruff, Gabriel A Hackebeil, Bethany L Nicholson, and John D Siirola. *Pyomo-optimization modeling in python*, volume 67. Springer, 2017.
[41] Fabian Pedregosa, Gaël Varoquaux, Alexandre Gramfort, Vincent Michel, Bertrand Thirion, Olivier Grisel, Mathieu Blondel, Peter Prettenhofer, Ron Weiss, Vincent Dubourg, et al. Scikit-learn: Machine learning in python. *Journal of machine Learning research*, 12:2825–2830, 2011.

Appendix A. Gantt chart for instance A-C

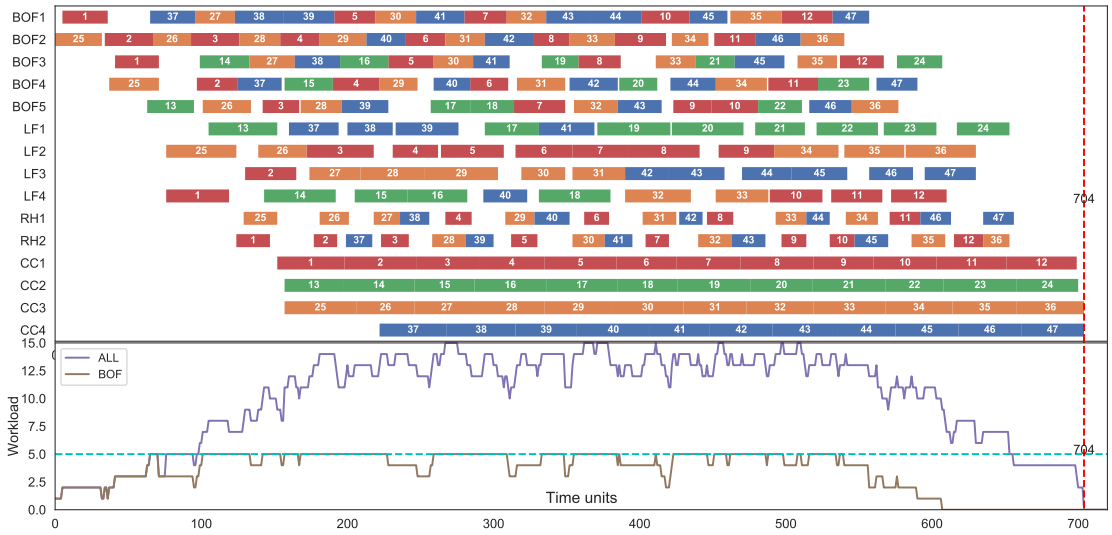

(a) Scenario 1: $C_{\max} = 704, W_{\text{tot}} = 304$

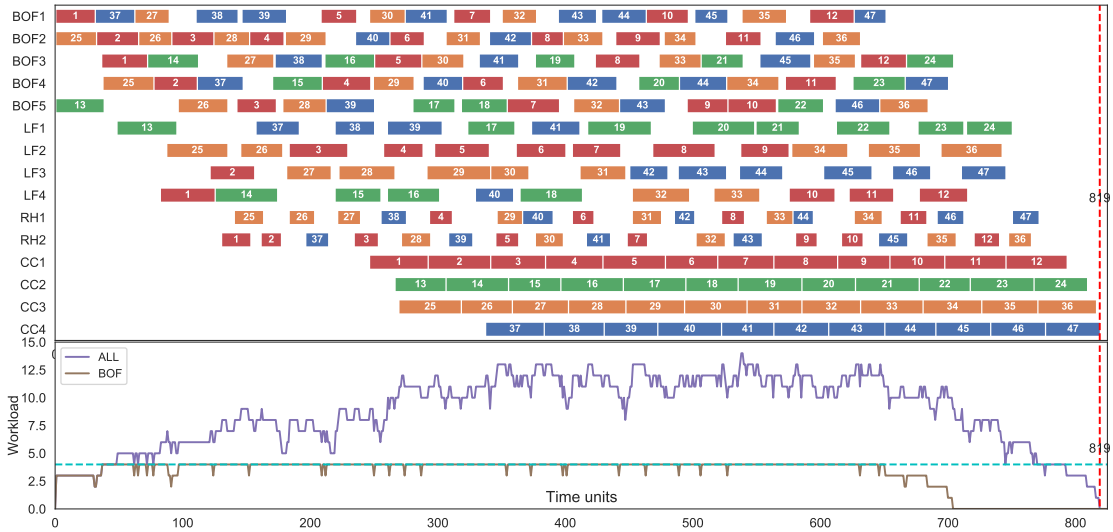

(b) Scenario 2:$C_{\max} = 819, W_{\text{tot}} = 3642$

Fig. A1: Gantt chart of Instance A

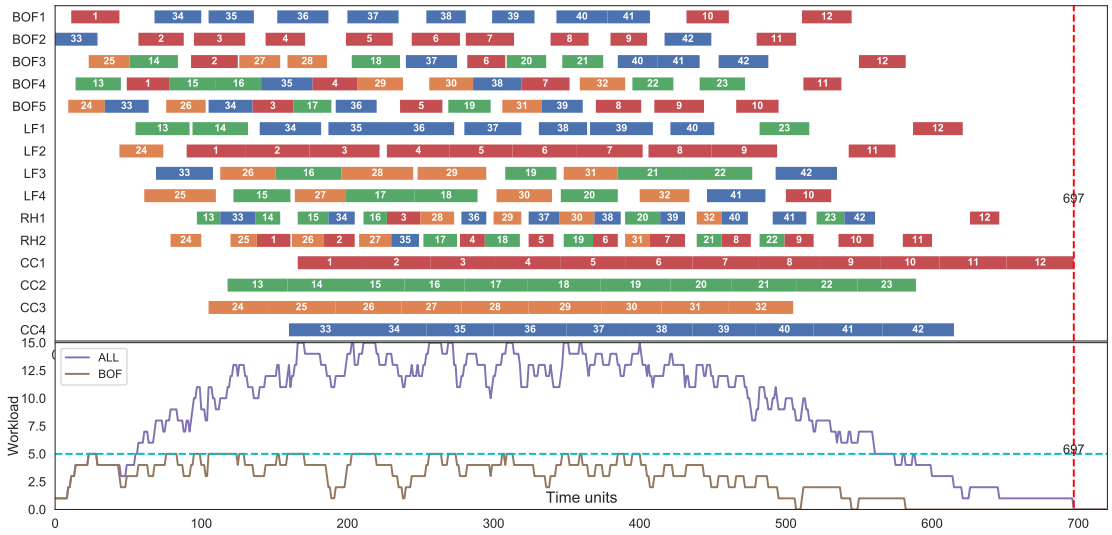

(a) Scenario 1: $C_{\max} = 697, W_{\text{tot}} = 60$

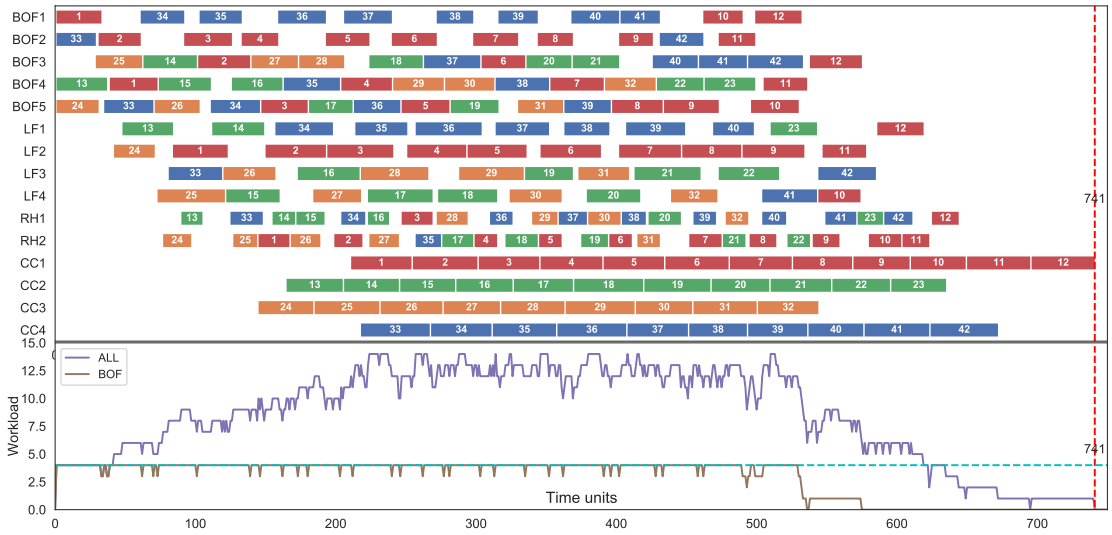

(b) Scenario 2: $C_{\max} = 741, W_{\text{tot}} = 1551$

Fig. A2: Gantt chart of Instance B

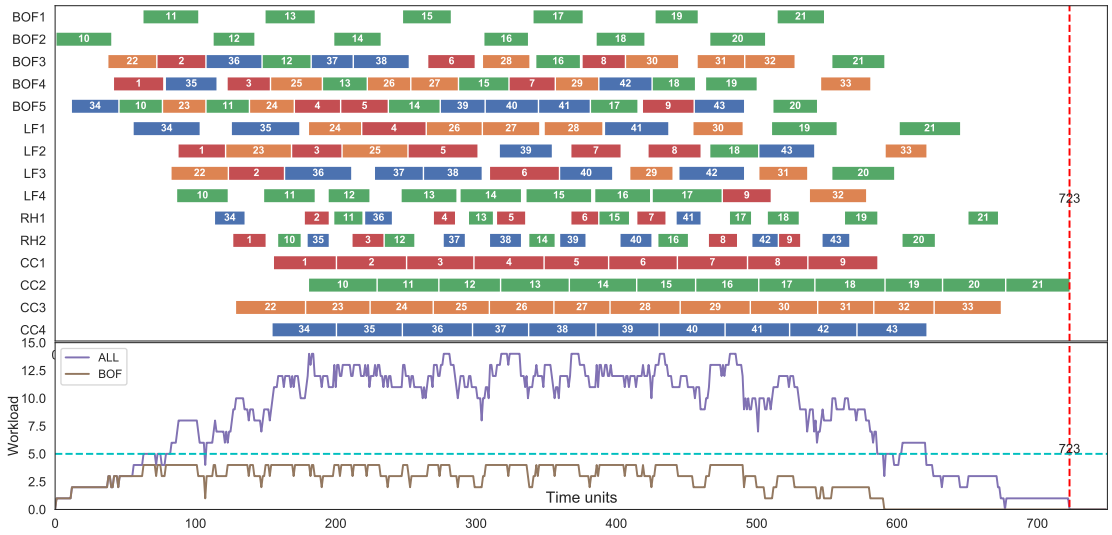

(a) Scenario 1: $C_{\max} = 723, W_{\text{tot}} = 455$

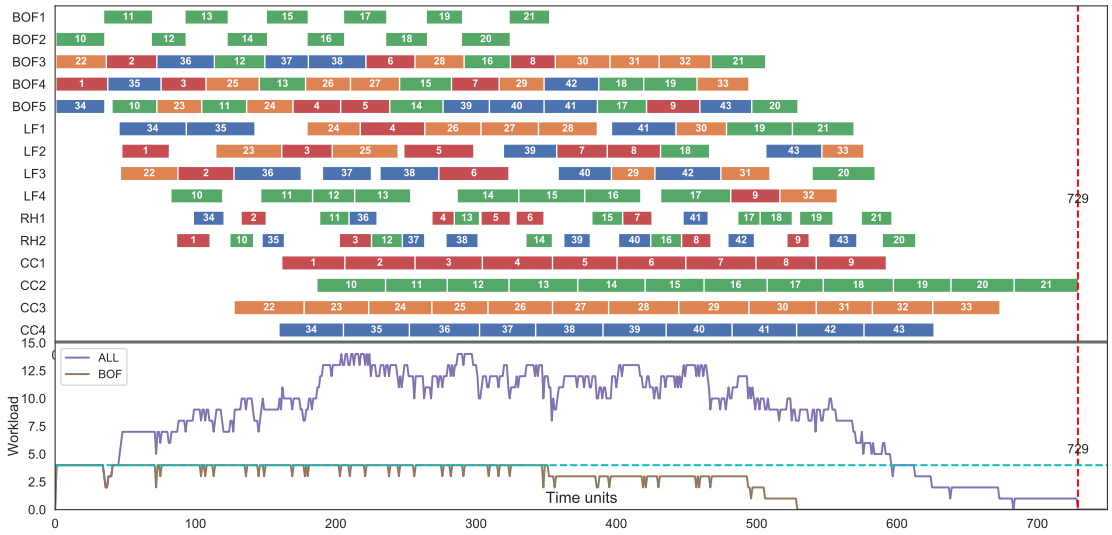

(b) Scenario 2: $C_{\max} = 729, W_{\text{tot}} = 2841$

Fig. A3: Gantt chart of Instance C

Appendix B. Demand curve for instance A-C

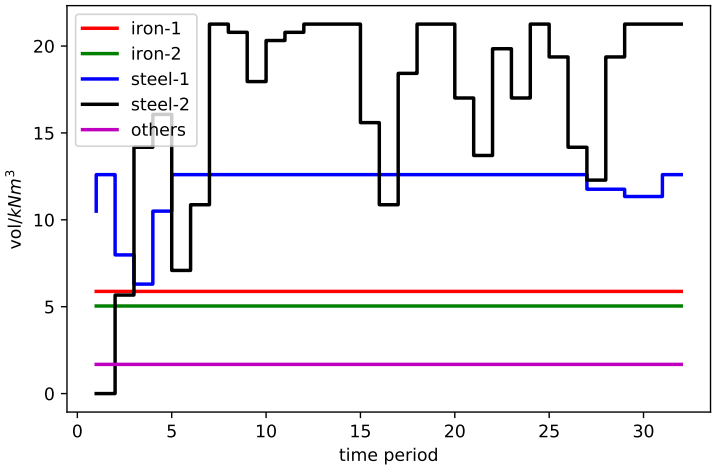

(a) Scenario 1

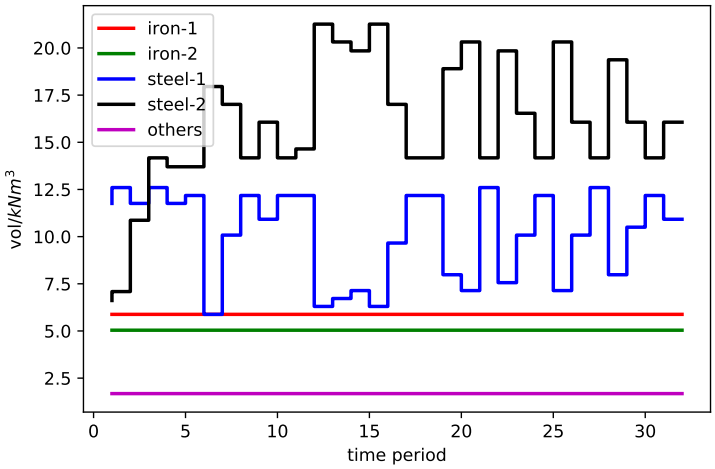

(b) Scenario 2

Fig. B1: Oxygen demand curve of Instance A

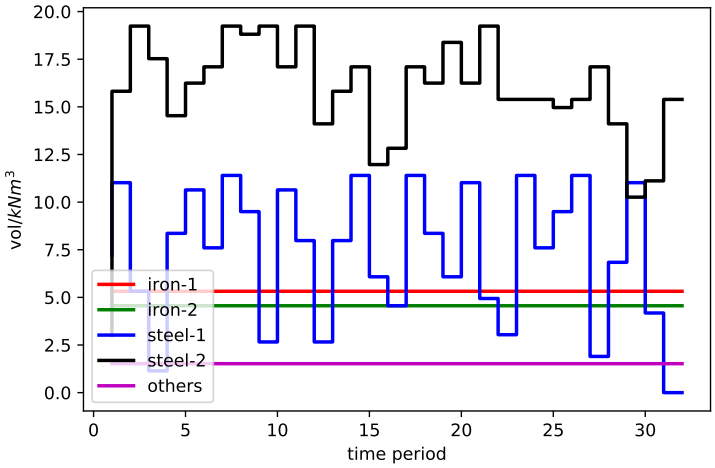

(a) Scenario 1

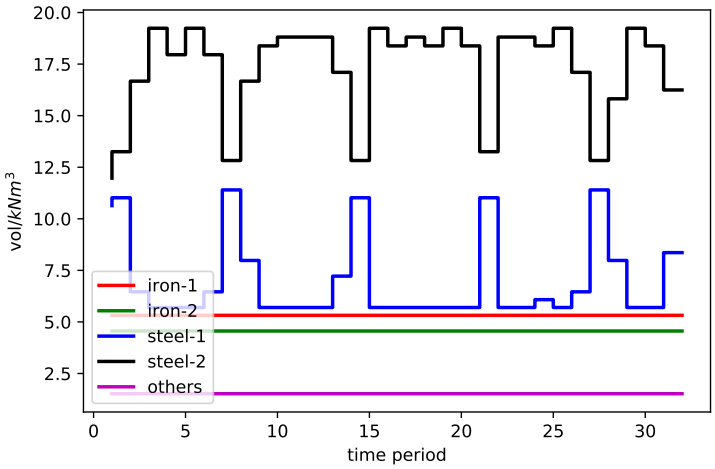

(b) Scenario 2

Fig. B2: Oxygen demand curve of Instance B

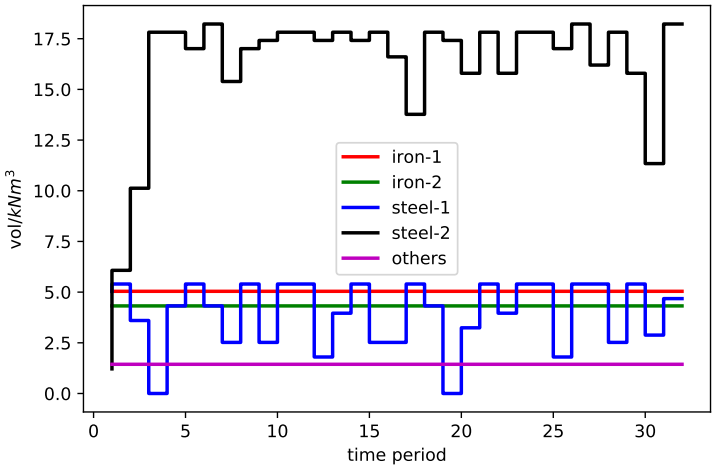

(a) Scenario 1

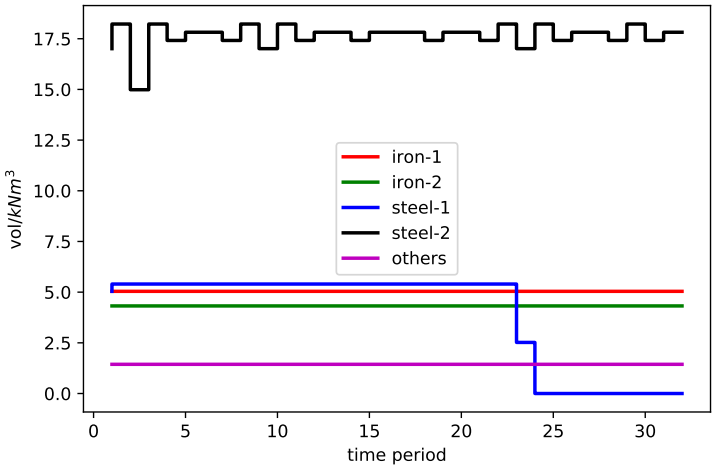

(b) Scenario 2

Fig. B3: Oxygen demand curve of Instance C